

Sherbrooke, Québec, January 21, 2016

**To:**

Prof. Claude Duguay, Handling Editor

**Object:** Revision of Manuscript tc-2015-173

Manuscript Title: Microwave snow emission modeling uncertainties in boreal and subarctic environments.

Dear Editor,

Please find attached to this letter the revisions to the manuscript entitled: "Microwave snow emission modeling uncertainties in boreal and subarctic environments".

We would like to thank the reviewer for comments which were useful in producing an improved manuscript. We answered to all reviewer comments.

Please, do not hesitate to contact me if you have any further questions or comments, or if anything is missing from the submission of the revised manuscript.

Regards,

---

Alexandre Roy  
Ph.D in Remote Sensing  
Centre d'applications et de recherches en télédétection (CARTEL)  
Département de Géomatique Appliquée  
Université de Sherbrooke  
Sherbrooke, Québec, J1K 2R1  
Office # A6-1028  
Tel.: 819-821-8000 ext.: 62956  
Fax: 819-821-7944  
Alexandre.R.Roy@USherbrooke.ca

In blue: Reviewer's comments. To better identify the questions, we added reference symbols: R= Reviewer ; C = Comments;

In black: Answers to reviewer

(Page): the pages where modification to text were added

*In black and italic: Modification added to text.*

**Reviewer #1 (Comments):**

This paper concerns the modeling of microwave radiation from snow with DMRT-ML, to quantify the simulation sensitivity to parameter uncertainty. This is the most complete study to date due to the consideration of the forest contribution as well as density, grain size, ice lens and soil roughness variability or uncertainty, with the latter effects providing no surprises based on other similar studies. In addition, to my knowledge, this is the first study to look at the effects of the bridging assumption between low and high density snow in the context of real data. The nominal simulations are considered to include a given grain scale factor, the density bridging assumption and appropriate treatment of ice lenses, before looking at other effects, which is a logical approach to take.

R1-C1 : This study looks at 3 different sites within the Canadian sub-Arctic, which gives a range of snowpack properties, but makes the paper somewhat hard to read. Due to the wide range of measurement locations, a figure with the sites indicated on a vegetation map would be useful.

We inserted a map of the 3 locations with the Land Cover of Canada 2005 (Latifovic et al., 2004) in background.

R1-C2 : In the James Bay measurements, the mean snow density from January to February decreased, and with minimal increase in grain size. Is this expected for this site? Is this due to the influence of recent precipitation, or spatial variability in the measurement locations? Also, how is the mean grain radius calculated?

The lower density in February is related to an error in density calculation. The snow density calculation was done considering the ice lenses. All the corrections were made (See also R2-C6)

The mean grain radius is the mean  $R_{opt}$  per layer weighted by the snow layer thickness. It is now mentioned in the text:

“During the JB<sub>Jan</sub> campaign, 16 open area sites were measured where the mean  $\rho_{snow}$  (*weighted by snow layers thickness excluding ice lenses*) of all snowpits was  $295.5 \text{ kg m}^{-3}$  and the mean  $R_{opt}$  (*weighted by snow layers thickness excluding ice lenses*) was 0.17 mm (Table 1).”

R1-C3 : Constant soil parameters from a different study were used here (section 2.2.3). The authors must comment on the applicability of these parameters to the sites chosen for this study. The experiment presented in section 3.2.1 considers the effect of the roughness of the soil, but not the permittivity, which governs the Fresnel reflectivity and

is a more fundamental parameter. The authors note this limitation later in the section, but I do not agree with their statement (pg 5732, line 15) that this does not affect their main goal. It may do, as the variability in the permittivity may cause greater snow TB variability than is possible to simulate with adjustment of the roughness alone. The authors should justify why a particular constant value of permittivity derived elsewhere is an appropriate assumption here or base the sensitivity on permittivity rather than roughness variability.

The parameters were inverted from independent angular measurement taken during the same campaign at James Bay. We thus clarify that point in Section 2.2.3:

“The values of  $\epsilon$ ,  $\sigma$  and  $\beta$  at 11, 19 and 37 GHz inverted by Montpetit et al. (2015) for frozen soil (Table 6) were used in this study. *Montpetit et al. (2013) used independent snow free ground-based radiometer angular measurements taken at James Bay site in 2013 (same campaign). The parameters were also validated over Umiujaq (same campaign) snow removal experiment.*”

Because we use minimal and maximal values of optimized  $\sigma$  the range of  $T_B$  variability of frozen ground is well represented. Also, the permittivity used were retrieved at the same site:

“However, one should be careful in interpreting these results as the optimization could also compensate for uncertainties in the permittivity of frozen ground. Nevertheless, *because the minimal and maximal values of optimized  $\sigma$  are taken*, this does not affect our main goal, which is to estimate the variability in snow-covered  $T_B$  introduced by the soil in the model. *Furthermore, as mentioned in Sect. 2.2.3, the permittivity used in this study were retrieved at the same site as this study.*”

R1-C4 : Pg 5730 line 9-11. This is really hard to see in the figure. There are multiple outliers that easily cover this range in the simulations, so this sentence should be more precise.

We add a dotted line in the Fig. 6 to clarify the point.

R1-C5 : Figure 6, right doesn't add much to the message of the paper and diverts attention as there are many figures in this paper. As it has already been summarised in a single sentence I would recommend removing the figure.

We removed the figure and change the paragraph:

“*To test the bridging parameterization (see Sect 2.2.2), we used 13 tundra sites from the Churchill tundra database (Roy et al., 2013), 4 from Umiujaq and 2 from the James Bay snowpits. In each case, at least one snow layer with a snow density higher than  $367 \text{ kg m}^{-3}$  (ice fraction of 0.4: Dierking et al., 2012) is used. For each of the 19 sites studied, simulations at 37 GHz (the most sensitive frequency to snow) with and without the bridging implementation were conducted (all input parameters kept the same). The bridging has a relatively modest impact on simulations with an improvement in the RMSE of between 2 and 4 K at tundra sites (Umiujaq and James Bay). The greatest improvements are found for deep drifted tundra snowpits where there is a very thick wind slab with high  $\rho_{\text{snow}}$  and small rounded grains are present at the top of the snowpack.*”

R1-C6 : Section 3.2.4. How was the density of ice lenses measured in the field and what was

the result (alternatively this comment may belong in the next section if ‘was attempted’ should be replaced with ‘was not attempted’).

We replaced for “*was not attempted*”.

Technical comments (R1):

pg 5724 line 6. Make clear that the SSA is per unit mass rather than per unit volume.

We clarified the units

pg 5724 line 15 and onwards. JB may be a better, easier to read acronym than BJ.

We changed all the acronyms.

pg 5726 line 22. As a scaling factor of 3.3 has been applied following previous work, presumably non-sticky grains are assumed in the DMRT-ML simulations. This should be stated.

We changes the sentence :

“As such, a scaling factor of  $\phi = 3.3$  assuming non-sticky snow grains from Roy et al. (2013) for the seasonal snowpack is thus applied to get an effective radius in the microwave range ( $R_{eff}$ )”

pg 5727 line 21. In setting ice lens thickness to 1cm, how are the thicknesses of the adjoining layers adjusted, or is the overall depth of the profile in the simulations allowed to differ from the measured depth?

We mentioned that in the text :

“To keep the same total snow depth, the adjoining layers were adjusted by removing 0.5 cm of the layer above and below the ice layer.”

pg 5728 line 11. This should be  $> 350$ , not  $< 350$ .

It was corrected

pg 5729 line 20. The bridging implementation was tested for simulations based on snowpit data rather than tested on snowpits themselves.

Done

pg 5734 line 12. gains -> grains

Done

lg 5736 line 11. weaker -> less

Done

## Reviewer #2 (Comments):

General comments The authors present a study assessing uncertainties in microwave emission modeling from snow covered ground, arising from uncertainties in assigning model inputs from in situ information. One model, the DMRT-ML by Picard et al. is applied for the purpose. A set of surface-based radiometer measurements is used as a reference to model predictions. While not very original, the paper contributes regardless to an important topic in snow remote sensing. The results of the paper should be useful especially in guiding data collections in future, large scale campaigns of snow cover using passive microwave radiometry. The paper is well written and clear. However, I have some questions regarding the methodology applied, and would suggest the authors revise some of their conclusions before publication. See detailed comments in the following.

R2-C1 : Abstract, lines 42-43 and several places later on. Based on what is in the end a rather limited dataset, you draw conclusions that variations in the emission of frozen soil has only a small effect on brightness temperature of snow covered terrain. You alleviate this conclusion somewhat in the discussion (723-732), but it comes out very strongly in the abstract, which I feel is misleading. It is, for instance, unclear if the sites you had contained multiple soil types or not; the 'frozen' permittivity of clay rich soils, for example, will be quite different from that of mineral soil types, due to the ability to store free water even in sub-zero conditions. Organic soils represent yet another different scenario, as well as soils with a high saline content. You only have to look at e.g. SMOS data during winter to see that there are variabilities during the winter which clearly arise from soils with a different permittivity. It would be good to better bring out the limitations already in the abstract (i.e. your experimental findings apply only to a certain soil type), if you wish to raise this point at all

We clarify the results in the abstract. :

"A snow excavation experiment -- where snow was removed from the ground to measure the microwave emission of bare frozen ground -- shows that small-scale spatial variability (*less than 1 km*) in the emission of frozen soil is small. Hence, *in our case of boreal organic soil*, variability in the emission of frozen soil has a small effect on snow-covered brightness temperature ( $T_B$ )."

We also clarify in the results section (the soil types were mentioned in Sect. 2.1.1) that the  $BJ_{Jan}$ -transect were made in an old gravel with mineral soil and, the other were made in organic boreal soil:

"The analysis of small-scale soil variability in modeling the  $T_B$  of snow-covered surfaces is conducted using the SEEx from the transect during the  $JB_{Jan}$  (*mineral soil*) and  $JB_{Feb}$  campaigns (*organic soil*)."

" $T_B$  variations of 0.5 K and 1.3 K were observed at the  $JB_{Jan}$ -transect site where the soil properties were more homogeneous (*mineral soil*), while a variation of 0.7 K to 3.8 K was measured at the  $JB_{Feb}$  site with *organic soil* (Table 8)."

R2-C2 : Abstract, lines 51-52, also later on: it is bit of a no-brainer that downwelling emission from trees affects the measured  $T_b$ . This is well known and it would simply be a mistake

not to include the downwelling canopy contribution – thus is a bit awkward to bring this out here. The absolute value of the  $T_b$  contribution, will be highly dependent on tree type and canopy conditions (frozen/thawed, snow covered/bare), as well as snow and soil reflectivity, thus I would refrain from giving a value here. If you insist, you should at least make it clear that this finding applies only to your study, test sites and the local conditions that prevailed.

From our knowledge, it is the first time that the contribution of forest emission reflected by the surface are quantified from ground-based radiometers. We think it is important to include in the abstract. We however mentioned in the abstract that the results are specific for our dataset:

“The results also show that, *in our study with the given boreal forest trees characteristics*, forest emission reflected by the surface can increase the  $T_b$  up to 40 K. *The forest contribution also varies with vegetation characteristic and a relationship between  $T_{B\text{down}}$  and the proportion of pixels occupied by vegetation (trees) in fisheye pictures was found.*”

R2-C3 : Introduction, lines 105-107 and elsewhere: Here, you claim to “quantify the sources of uncertainty in the DMRT-ML model”. However, in the previous paragraph, you point out the two basic contributions to simulation (not model!) uncertainty: 1) model physics going wrong 2) insufficient or inaccurate input information. To me, the whole paper is about assessing point 2), as is in fact also pointed out in the discussion (line 740-741). This is an important distinction and you should be careful with the wording throughout the paper. In my view a better wording here would be something along the lines of: “we aim to quantify the relative importance of uncertainties of in situ information, when simulating microwave TB with the DMRT-ML model”.

We clarify the main objective of the paper:

“Hence, this paper aims to better quantify the relative importance of different geophysical parameters and small-scale spatial variability when simulating microwave  $T_b$  with the Dense Media Radiative Theory-Multilayer model (DMRT-ML; Picard et al. 2013).”

We also clarify that point in the first sentence of Sect. 4 :

“This study presents a comprehensive analysis of the *geophysical parameters* contributing to uncertainty in DMRT-ML for snow-covered surfaces in boreal forest, subarctic and arctic environments.”

R2-C4 : Lines 111-112: sentence a little bit incomplete. Add something like “: : : snow emission modeling: inaccuracies in quantifying snow grains, snow density”

The proposed change was done

R2-C5 : Section 2.1, lines 163-165. Measuring SSA may be robust, but being a definition for optical wavelengths, how well is SSA related to the propagation of microwaves in snow? I’m sure the authors are aware of this ongoing discussion. You do not have to delve deep into the problem here, but at least the question and the related discussion should be acknowledged by citing some recent work by e.g. Mätzler, also justifying why you use SSA regardless of the acknowledged limitations.

To our knowledge, SSA is the only robust and objective metric that can be measured in situ. We are now working on a paper showing that SSA is a better metric than  $D_{\max}$ . We developed in the discussion on the justification of the use of SSA with some limitation.

“The error related to the physical simplifications in DMRT-ML was not investigated in this work, but our results suggest that the level of confidence of measurements is too low to test or significantly improve the DMRT-ML physics. *In this study, SSA was used because it is a robust and objective metric that can be measured effectively on the field. However, the derived  $R_{\text{opt}}$  metric used in DMRT-ML is related to an optical definition (Grenfell and Warren, 1999) and might not represent the grain for microwave wavelength (see Mätzler, 2002).* Further experiments on isolated snow layers as done by Wiesmann et al. (1998) but using new tools for snow microstructure parameterization could be applied to improve the physics of emission models. For example, more precise measurements of snow microstructure like X-ray tomography (Heggli et al., 2011) and the snow micro penetrometer (SMP) (Schneebeli et al., 1999; Proksch et al., 2015) could be the next step to improve the understanding of the physics in DMRT-ML (e.g., Lowe and Picard, 2015).”

R2-C6 : Tables 1-5: the STD values for snow density seem very high to me, especially for Tables 1&2. Can you check these? If the values are correct, do you have a reason for the high degree of variability?

The average density and standard deviation of snow density calculation included the ice lenses. The values were recalculated without the ice lenses to give a better view of the snowpack characteristics. The values were corrected in the text as well (See also R1-C2).

R2-C7 : Section 2.2.3, line 340: epsilon' is the conventional symbol for the real part of the dielectric permittivity. The Fresnel reflectivity depends on  $\langle \epsilon_{\text{r}} \rangle = \langle \epsilon' + j\epsilon'' \rangle$ . Is your epsilon' the real part of the soil permittivity (thus neglecting the imaginary part, a reasonable approximation for frozen soil), or the magnitude of the complex permittivity?

We clarify in the text that it is the real part of the soil permittivity:

“where  $\Gamma_{f,p}$  is the rough soil reflectivity at a frequency  $f$  and polarization  $p$  (H-pol or V-pol) by its smooth Fresnel reflectivity in H-Pol ( $\Gamma_{f,H}$ ), which depends on the incidence angle ( $\theta$ ) and the *real part of the soil permittivity* ( $\epsilon'$ ), weighted by an attenuation factor that depends on the standard deviation in height of the surface (soil roughness,  $\sigma$ ), the measured wavenumber ( $k$ ) and a polarization ratio dependency factor ( $\beta$ ).”

R2-C8 : Section 3.1.1., line 374-376: what is the fundamental reason for the simulation to go wrong, when the effect of ice lenses is not included? Is it not very informative to just state that “improved simulations” are achieved with ice lenses. In other words, what is the physical effect that the ice lenses manage to simulate, which was lacking in the original simulation? This should be explained.

We clarify that the ice lenses inclusion allows taking into account its strong reflectivity:

These results show that a simple ice lens implementation in DMRT-ML helps *to simulate the*

*strong reflection component of ice lenses (decrease of snowpack emissivity), leading to improved simulations of  $T_B$ .*

R2-C9 : Still on ice lenses: can you elaborate your statement on line 380: what, in your view, are the reasons for the limited range of simulated values versus observations, if this is related to ice lenses. Coherence effects not accounted for by DMRT? Or, can this be something different (the soil perhaps?). coherence is mentioned in the discussion, but something could be pointed out here.

We chose not to elaborate on the reason for the limited range because it is well discussed in Sect. 3.2.4 and Sect. 4. But after review we add some sentences to start the discussion on that point:

“This feature suggests some limitations of ice lens and/or snow layering modeling in DMRT-ML that can be related to the fact that coherence effect is not taken into account. Note that this underestimation of  $T_B$  spatial variability is not related to the soil as demonstrated in Sect. 3.2.1. The modeling uncertainties related to ice lenses will be discussed more specifically in Sect. 3.2.4.”

R2-C10 : Lines 417-418: rather than ‘5-10 K’ and ‘10-20 K’, give precise numbers. Note e.g. that RMSE at 11H exceeds 20 K, and RMSE for 19V lower than 5 K.

The numbers were updated:

“The RMSE values oscillate between 7.8 and 21.5 K at H-pol (Table 7). Since V-pol is less affected by layering in the snowpack at 11 GHz and 19 GHz, the RMSE are generally lower (between 3.5 and 14.4 K), while the RMSE at 37 GHz are similar at V-pol and H-pol.”

R2-C11 : Figure8: error bars in scatterplot not very informative, they only make the symbols hard to read. I suggest to remove these

We think that the error bars allow showing that the effect of soil emission small-scale spatial variability has a very low impact on  $T_B$ . For this reason we think it worth to keep the error bars.

R2-C12 : Section 3.2.2: summing of errors; is the 12% error in SSA considered random, or systematic? I think random? Then, you should rather perform a sum-of-squares addition of the errors, depending on how many measurements were used for a given snowpit [e.g. for three SSA measurements used in a sim:  $err\_tot = \sqrt{err\_1^2 + err\_2^2 + err\_3^2} = 0.21$ ]. I suggest to redo the analysis (Fig9, Table 9) in this fashion.

In our case, the error of 12% is added to the SSA of each layer of snowpack. Hence, the  $T_B$  error account for the sum of the error of each layer. The error in  $T_B$  resulting from the uncertainties in SSA measurements for each layer correspond to an integrated errors which are not independent from each other, since there are multiple scattering between the layers. In the Table 9, we show the extreme variations in  $T_B$  for the extreme cases where all the errors in SSA are in the same way (all positive + 12%, and all negative -12%). This gives the limit cases. In reality, one can assume a random error in SSA measurements between + and - 12% to calculate  $T_B$  with a random error applied on SSA ( $T_{Bsimrand}$ ). We assessed the average variation in  $T_B$  ( $T_{Bsim} - T_{Bsimrand}$ ) resulting from 100 runs with random error ( $\pm 12$ ) in SSA for each layers of every snowpits. The

Table R.1 below shows the results. As expected, the variation is significantly lower than those shown in Table 9 of the paper. This Table gives the lower limits, while the Table 9 gives the highest limit.

**Table R.1:**  $T_B$  variation ( $T_{B\text{sim}} - T_{B\text{simrand}}$ ) associated with random error ( $\pm 12\%$ ) applied to each SSA measurements (average of 100 runs)

|     | JB <sub>Jan</sub> | JB <sub>Feb</sub> | JB <sub>Mar</sub> | UMI |
|-----|-------------------|-------------------|-------------------|-----|
| 11H | 0.0               | 0.1               | 0.1               | 0.0 |
| 11V | 0.0               | 0.1               | 0.1               | 0.0 |
| 19H | 0.3               | 0.6               | 0.8               | 0.3 |
| 19V | 0.3               | 0.6               | 0.9               | 0.3 |
| 37H | 2.1               | 2.0               | 1.7               | 1.2 |
| 37V | 2.7               | 2.4               | 2.1               | 1.4 |

We added the following sentence in the text:

*“We assessed average variation in  $T_B$  resulting from 100 runs with random error between  $\pm 12\%$  applied to SSA for each layer and snowpit. As expected, the results show that the variations between initial simulation and simulation with random error on SSA are significantly lower than those shown in Table 9. With random error applied on SSA measurements, the variations are lower than 1 K at 11 and 19 GHz, and between 2 and 3 K at 37 GHz. These values give the lower limits of  $T_B$  error related to SSA uncertainties, while values in Table 9 give the highest limit of the variation in  $T_B$ .”*

R2-C13 : Line 595: I think you mean “was NOT attempted”.

It was changed.

R2-C14 : Conclusions, p26, lines 760-765. You could cite Derksen (2008) in the discussion here, who suggested the use of 11-19 GHz in place of 19-37 GHz for deep snow to alleviate saturation effects at 37 GHz.

We added a sentence on the possibility to use 11-19 instead of 19-37:

*“This could be of interest for the SWE retrieval approach, knowing that 19 GHz  $T_B$  becomes sensitive to snow when snow grains become larger. As proposed in Derksen (2008) 11 and 19 GHz frequencies could be usefull for SWE retrievals for deep snow to overcome the problem of saturation at 37 GHz (see Rosenfeld and Grody, 2000). At 11 GHz, snow is almost transparent throughout the winter demonstrating the utility of this band for monitoring soil conditions (phase, temperature) under the snow (Kohn and Royer, 2010).”*

Editorial P11, line 333 delete “therefore”

Done

1                   **Microwave snow emission modeling uncertainties in boreal and**  
2                   **subarctic environments**

5                   A. Roy<sup>a-b\*</sup>, A. Royer<sup>a-b</sup>, O. St-Jean-Rondeau<sup>a-b</sup>, B. Montpetit<sup>a</sup>, G. Picard<sup>c</sup>, A. Mavrovic<sup>a</sup>,  
6                   N. Marchand<sup>a-b-c</sup> and A. Langlois<sup>a-b</sup>

7

8

9                   <sup>a</sup> Centre d'Applications et de Recherches en Télédétection (CARTEL), Université de  
10                   Sherbrooke, 2500 boul. Université, Sherbrooke, QC, Canada, J1K 2R1.

11                   <sup>b</sup>Centre d'études Nordiques, Québec, Canada

12                   <sup>c</sup> Université Grenoble Alpes - CNRS, LGGE UMR5183, 38041 Grenoble, France

13

14

15

16                   *Revised manuscript for publication in The Cryosphere*

17

18

19

20                   \*Corresponding author:

21                   Alexandre Roy

22                   Ph. D. in Remote Sensing

23                   Centre d'applications et de recherches en télédétection (CARTEL)

24                   Département de Géomatique Appliquée

25                   Université de Sherbrooke

26                   Sherbrooke, Québec, Canada, J1K 2R1

27                   Office # A4-280

28                   Tel.: 1-819-821-8000 ext.: 61904

29                   Fax: 1-819-821-7944

30                   Alexandre.R.Roy@USherbrooke.ca

31 **Abstract.**

32  
33 This study aims to better understand and quantify the uncertainties in microwave snow  
34 emission models using the Dense Media Radiative Theory-Multilayer model (DMRT-  
35 ML) with in-situ measurements of snow properties. We use surface-based radiometric  
36 measurements at 10.67, 19 and 37 GHz in boreal forest and subarctic environments and a  
37 new in situ dataset of measurements of snow properties (profiles of density, snow grain  
38 size and temperature, soil characterization and ice lens detection) acquired in the James  
39 Bay and Umiujaq regions of Northern Québec, Canada. A snow excavation experiment --  
40 where snow was removed from the ground to measure the microwave emission of bare  
41 frozen ground -- shows that small-scale spatial variability (**less than 1 km**) in the emission  
42 of frozen soil is small. Hence, **in our case of boreal organic soil**, variability in the  
43 emission of frozen soil has a small effect on snow-covered brightness temperature ( $T_B$ ).  
44 Grain size and density measurement errors can explain the errors at 37 GHz, while the  
45 sensitivity of  $T_B$  at 19 GHz to snow increases during the winter because of the snow grain  
46 growth that leads to scattering. Furthermore, the inclusion of observed ice lenses in  
47 DMRT-ML leads to significant improvements in the simulations at horizontal  
48 polarization (H-pol) for the three frequencies (up to 20 K of root mean square error).  
49 However, the representation of the spatial variability of  $T_B$  remains poor at 10.67 and 19  
50 GHz at H-pol given the spatial variability of ice lens characteristics and the difficulty in  
51 simulating snowpack stratigraphy related to the snow crust. The results also show that, **in**  
52 **our study with the given forest characteristics**, forest emission reflected by the surface  
53 can increase the  $T_B$  up to 40 K. **The forest contribution varies with vegetation**  
54 **characteristic and a relationship between the downwelling contribution of the vegetation**  
55 **and the proportion of pixels occupied by vegetation (trees) in fisheye pictures was found.**  
56 We perform a comprehensive analysis of the components that contribute to the snow-  
57 covered microwave signal, which will help to develop DMRT-ML and to improve the  
58 required field measurements. The analysis shows that a better consideration of ice lenses  
59 and snow crusts is essential to improve  $T_B$  simulations in boreal forest and subarctic  
60 environments.

61  
62 Keywords: DMRT-ML, snow, vegetation, ice lenses, soil emissivity, microwave

63  
64 **1. Introduction**

65  
66 Seasonal snow cover plays an important role in the surface energy balance (Armstrong  
67 and Brun, 2008). Snow, with its low thermal conductivity, has an insulating effect on  
68 soils, which can greatly influence vegetation (Liston et al., 2002) and the development of  
69 active layers in permafrost (Gouttevin et al., 2012; Shurr et al., 2013). Snow water  
70 equivalent (SWE) is also a key variable in the high latitude water cycle (Déry et al.,  
71 2009) and is important for dam management and hydroelectricity production (Roy et al.,  
72 2010). Conventional in situ observations, such as from meteorological stations, are often  
73 inadequate to monitor seasonal snow evolution given the sparse distribution of stations in  
74 northern regions. Furthermore, point measurements are subject to local scale variability  
75 and may not represent the prevailing regional conditions. For these reasons, monitoring  
76 SWE from satellite passive microwave (PMW) observations has been the subject of

77 numerous studies for nearly three decades (e.g., Chang et al. 1987; Goodison et al., 1986;  
78 Derksen, 2008). The PMW are sensitive to SWE, but also have the advantage of  
79 providing observations at a synoptic scale in any weather conditions: images are available  
80 at least twice a day for the northern regions. However, estimation of SWE is not  
81 straightforward and existing empirical algorithms based on linear relationships between  
82 SWE and spectral  $T_B$  are often inaccurate due to seasonal snow grain metamorphism  
83 (Rosenfeld and Grody, 2000). Vegetation contributions are also an important factor with  
84 large interannual variability (Roy et al., 2015), which is not captured by these algorithms.  
85 Hence, radiative transfer models (RTM) including microwave snow emission models  
86 (MSEM) can be used to take into account the different contributions to the microwave  
87 signal and the interannual variability of critical geophysical parameters. The GlobSnow2  
88 SWE retrieval algorithm (Takala et al., 2011) uses an assimilation scheme combining  
89 PMW observations constrained with kriged measurements of snow depth from  
90 meteorological stations. This method, however, has some limitations in remote areas  
91 where snow measurements are sparse, thus highlighting the need to improve MSEM  
92 performance in such a way that SWE retrievals can be achieved without in situ  
93 observations (Larue et al., 2015).

94  
95 At the satellite scale, PMW observations generally have a coarse spatial resolution (more  
96 than 10 km x 10 km). Nevertheless, spatial heterogeneity within PMW pixels becomes a  
97 limitation for the development and validation of MSEM because contributions from  
98 snow, vegetation and lakes are difficult to decouple. Therefore, surface-based  
99 radiometers (SBR) are used to better understand and isolate the contribution of snow-  
100 covered surfaces. However, independently of MSEM used and seasonal snow type, the  
101 comparison between simulated  $T_B$  and SBR observations leads to errors in the order of 10  
102 K (Roy et al., 2013; Montpetit et al., 2013; Derksen et al., 2012; Kontu and Pulliainen,  
103 2010; Lemmetyinen et al., 2010; Lemmetyinen et al., 2015; Durand et al., 2008). From  
104 SBR measurements, these errors can be explained by 1) MSEM physical simplification  
105 (Tedesco and Kim, 2006) and 2) small scale variability and uncertainty in measurements  
106 of geophysical parameters.

107  
108 Hence, this paper aims to better quantify the relative importance of different geophysical  
109 parameters and small-scale spatial variability when simulating microwave  $T_B$  with the  
110 Dense Media Radiative Theory-Multilayer model (DMRT-ML; Picard et al. 2013). The  
111 study is based on a new and unique database including SBR measurements at three  
112 microwave frequencies (37, 19 and 10.67 GHz) in boreal and subarctic environments.  
113 The study assesses a wide range of contributions that could lead to uncertainties in  
114 ground-based microwave snow emission modeling: snow grains, snow density, soil  
115 roughness, ice lenses (IL) and vegetation. More specifically, the objectives of the study  
116 are:

117  
118 1. Validate the snow emission modeling, including recent improvements accounting for  
119 ice lenses (Montpetit et al., 2013) and snow density in the  $367\text{--}550 \text{ kg m}^{-3}$  range  
120 (Dierking et al., 2012).

121

122 2. Evaluate the different contributions to modeling uncertainty (snow grains, snow  
 123 density, ice lenses, soil and vegetation measurements).

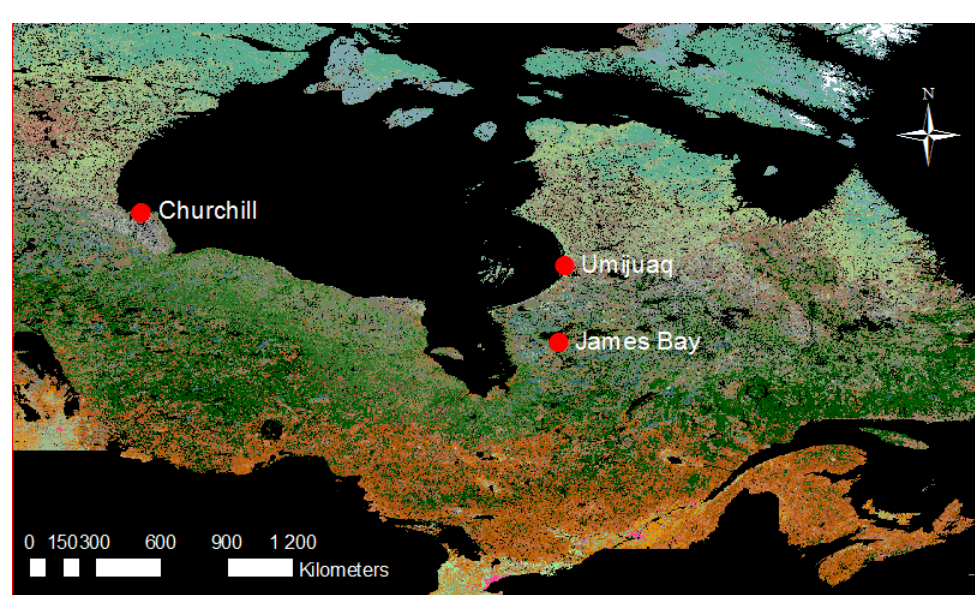
124 3. Quantify the sensitivity of simulated  $T_B$  to the measurement accuracy.

125

126 **2. Method**

127 **2.1 Sites and Data**

131 Surface-based radiometer observations were acquired during the 2010 field campaign at  
 132 the Churchill Northern Studies Center (Northern Manitoba) (see Roy et al., 2013 for a  
 133 detailed description of the field campaign) and during four subsequent field campaigns in  
 134 Northern Québec, Canada: three in James Bay ( $53^{\circ}26'N$ ;  $76^{\circ}46'W$ , 186 m a.s.l) in winter  
 135 2013 and one campaign in Umiujaq ( $56^{\circ}33'N$ ,  $76^{\circ}30'W$ , 74 m a.s.l) in winter 2014 (Fig.  
 136 1). All these campaign allow covering a wide range of environmental conditions from  
 137 dense boreal forest to open tundra for a total of 51 snowpits (excluding the Churchill  
 138 snowpits).



140  
 141 Fig. 1. Location of field campaigns. Background: Land Cover of Canada (Latifovic et al.,  
 142 2004)

Comment [AR1]: New figure

143  $T_B$  measurements were acquired at 37, 19 and 10.67 GHz in both vertical (V-pol) and  
 144 horizontal (H-pol) polarizations at a height of approximately 1.5 m above the ground and  
 145 at an angle of  $55^{\circ}$  with the PR-series Surface-Based Radiometers from Radiometrics  
 146 Corporation (Langlois, 2015) (hereinafter, the 10.67 GHz SBR is noted 11 GHz for  
 147 simplicity). With a beam width of  $6^{\circ}$  for 37 and 19 GHz SBR, the footprint of the  
 148 measurements at the snow surface was approximately  $0.6 \text{ m} \times 0.6 \text{ m}$ . The 11 GHz beam  
 149 width is  $8^{\circ}$  with a footprint of about  $0.8 \times 0.8 \text{ m}$ . In the worst case, the measurement error  
 150

151 for the calibration target was estimated at 2 K. The radiometers were calibrated before  
152 and after each field campaign using ambient (black body) and cold (liquid nitrogen)  
153 targets.

154 Within the footprint of every SBR observation, profiles of snow temperature, snow  
155 density ( $\rho_{\text{snow}}$  in  $\text{kg m}^{-3}$ ) and specific surface area (SSA in  $\text{m}^2 \text{kg}^{-1}$ ) were taken at a  
156 vertical resolution between 3 and 5 cm. Visual stratigraphy assessment of the main snow  
157 layers/features, including ice lenses, was conducted. The density was measured using a  
158 185-cm<sup>3</sup> density cutter, and samples were weighed with a 100-g Pesola light series scale  
159 with an accuracy of 0.5 g. The snow temperature and soil temperature were measured  
160 with a Traceable 2000 digital temperature probe ( $\pm 0.1$  °C). The SSA was measured with  
161 the shortwave InfraRed Integrating Sphere (IRIS) system (Montpetit et al., 2012) at the  
162 James Bay site and using the Dual Frequency Integrating Sphere for Snow SSA  
163 measurement (DUFISSS: Gallet et al., 2009) in Umiujaq. Both instruments exploit the  
164 relationship between the SWIR snow reflectance and the SSA (Kokhanovsky and Zege,  
165 2004) based on the principle described in Gallet et al. (2009). From SSA measurements,  
166 the optical radius of the snow grain ( $R_{\text{opt}}$ ) was calculated by:  
167

$$168 \quad R_{\text{opt}} = \frac{3}{\rho_{\text{ice}} \text{SSA}} \quad (1)$$

170 where  $\rho_{\text{ice}}$  is the ice density = 917 kg m<sup>-3</sup>. The SSA is one of the most robust and  
171 objective approaches to measure a parameter related to the size of snow grains in the  
172 field. The error for SSA measurements was estimated to be 12% (Gallet et al., 2009).

### 173 2.1.1 James Bay, Québec, Canada

174 Three intensive measurement periods were conducted during the 2013 winter season in  
175 the James Bay area, Québec, in January (8<sup>th</sup> to 12<sup>th</sup>: JB<sub>Jan</sub>), February (12<sup>th</sup> to 17<sup>th</sup>: JB<sub>Feb</sub>)  
176 and March (19<sup>th</sup> to 23<sup>th</sup>: JB<sub>Mar</sub>) (Tables 1, 2 and 3). The sites were in a typical boreal  
177 forest environment, but most of the measurements were conducted in clearings with  
178 minimal influence of the environment (topography, vegetation) on the measured  $T_B$ .  
179 However, 15 measurements, spanning across the three campaigns, were conducted in  
180 forested areas and were treated separately to specifically investigate the contribution of  
181 vegetation on the ground-based measurements (Table 4). Several snow excavation  
182 experiments (denoted SEex) were also conducted where snow was removed to measure  
183 frozen ground emission. During SEex, large snowpits were dug (about 3 m x 3 m wide)  
184 and the snow walls removed to eliminate snow wall emission reflected on the ground. At  
185 all sites, the soil (described below) was frozen at least to a depth of 10 cm.  
186

187 During the JB<sub>Jan</sub> campaign, 16 open area sites were measured where the mean  $\rho_{\text{snow}}$   
188 (weighted by snow layers thickness excluding ice lenses) of all snowpits was 218.3 kg m<sup>-3</sup>  
189 and the mean  $R_{\text{opt}}$  (weighted by snow layers thickness excluding ice lenses) was 0.17  
190 mm (Table 1). Snowpits JB<sub>Jan</sub>-1 to JB<sub>Jan</sub>-5 were located in forest clearings where the soil  
191 composition mainly consisted of organic matter. On January 9<sup>th</sup>, a transect of 11 snowpits  
192 (JB<sub>Jan</sub>-6.1 to JB<sub>Jan</sub>-6.11, each separated by 3 m) was conducted in an old gravel pit  
193

196 (mostly mineral soil). Five SEex were also conducted in the 30 m transect. One to two ice  
 197 lenses of about 0.5 to 1 cm were observed in all snowpits, buried at depths of 10 and 30  
 198 cm.

199

200 **Table 1.** Average snow property values with standard deviation (in parentheses) at James  
 201 Bay (JB) sites in January. Values are provided for snow depth (SD m); mean snowpack  
 202 temperature ( $T_{\text{snow}}$ ); bulk density ( $\rho_{\text{snow}}$ ); mean optical radius ( $R_{\text{opt}}$ ); soil/snow temperature  
 203 ( $T_{\text{soil}}$ ); number of observed ice lenses (IL); and ‘bridging’ (B) indicates the presence of a  
 204 snow layer with a density within the bridging ice fraction limits (see Sect. 2.2.2).

| SP                     | Type   | SD (cm) | $T_{\text{snow}}$ (K) | $\rho_{\text{snow}}$ ( $\text{kg m}^{-3}$ ) | $R_{\text{opt}}$ (mm) | $T_{\text{soil}}$ (K) | IL | B | Date       |
|------------------------|--|---------|-----------------------|---|-----------------------|-----------------------|----|---|------------|
| JB <sub>an</sub> -1    | Forest clearing<br>Organic soil                              | 37      | 259.9 (4.8)           | 220.7 (37.4)                                | 0.19 (0.09)           | 272.3                 | 1  |   | 07-01-2013 |
| JB <sub>an</sub> -2    |  | 43      | 265.3 (3.4)           | 196.3 (40.4)                                | 0.15 (0.07)           | 272.0                 | 1  |   | 08-01-2013 |
| JB <sub>an</sub> -3    |  | 48      | 264.8 (4.2)           | 241.1 (37.2)                                | 0.20 (0.10)           | 272.6                 | 1  |   | 08-01-2013 |
| JB <sub>an</sub> -4    |  | 48      | 264.9 (3.6)           | 212.8 (48.5)                                | 0.17 (0.09)           | 272.3                 | 1  |   | 08-01-2013 |
| JB <sub>an</sub> -5    |  | 62      | 267.5 (1.8)           | 220.8 (45.9)                                | 0.15 (0.08)           | 272.4                 | 1  |   | 11-01-2013 |
| JB <sub>an</sub> -6.1  | Old gravel pit<br>Mineral soil<br>JB <sub>an</sub> -transect | 51      | 266.8 (2.4)           | 223.4 (39.6)                                | 0.17 (0.08)           | 271.5                 | 1  |   | 09-01-2013 |
| JB <sub>an</sub> -6.2  |  | 52      | 267.4 (2.4)           | 240.1 (42.5)                                | 0.18 (0.08)           | 271.5                 | 1  |   | 09-01-2013 |
| JB <sub>an</sub> -6.3  |  | 43      | 266.5 (1.4)           | 212.8 (34.9)                                | 0.17 (0.08)           | 271.3                 | 1  |   | 09-01-2013 |
| JB <sub>an</sub> -6.4  |  | 45      | 268.0 (2.3)           | 204.3 (37.8)                                | 0.18 (0.09)           | 272.1                 | 1  |   | 09-01-2013 |
| JB <sub>an</sub> -6.5  |  | 53      | 267.2 (2.6)           | 244.5 (40.4)                                | 0.16 (0.09)           | 272.6                 | 1  |   | 09-01-2013 |
| JB <sub>an</sub> -6.6  |  | 51      | 267.0 (2.2)           | 224.4 (38.5)                                | 0.18 (0.09)           | 272.0                 | 1  |   | 09-01-2013 |
| JB <sub>an</sub> -6.7  |  | 47      | 267.2 (2.0)           | 220.1 (34.5)                                | 0.16 (0.10)           | 271.6                 | 2  |   | 09-01-2013 |
| JB <sub>an</sub> -6.8  |  | 47      | 267.5 (2.3)           | 205.4 (36.5)                                | 0.14 (0.08)           | 271.8                 | 2  |   | 09-01-2013 |
| JB <sub>an</sub> -6.9  |  | 46      | 267.1 (1.8)           | 209.4 (32.0)                                | 0.16 (0.10)           | 271.1                 | 2  |   | 09-01-2013 |
| JB <sub>an</sub> -6.10 |  | 45      | 266.7 (1.5)           | 202.6 (23.8)                                | 0.14 (0.07)           | 270.3                 | 1  |   | 09-01-2013 |
| JB <sub>an</sub> -6.11 |  | 40      | 266.8 (1.2)           | 214.7 (24.2)                                | 0.17 (0.10)           | 269.6                 | 1  |   | 09-01-2013 |

205

206 Nine snowpits were dug during the February campaign (Table 2), with a mean  $\rho_{\text{snow}}$  of  
 207 225.2  $\text{kg m}^{-3}$  and a mean  $R_{\text{opt}}$  of 0.18 mm. All snowpits were conducted in clearings with  
 208 frozen organic soil. On the 15<sup>th</sup> of February, for a transect of seven snowpits, a complete  
 209 set of measurements was taken for each snowpit (SP). An ice lens at a depth of 30 cm  
 210 was observed at each SP. In addition to SP measurements, two SEex were conducted in  
 211 the transect and two others in JB<sub>Feb-1</sub> and JB<sub>Feb-2</sub>.

212

213 **Table 2.** Same as Table 1, but for James Bay sites in February (JB<sub>Feb</sub>).

| SP                     | Type                            | SD (cm) | $T_{\text{snow}}$ (K) | $\rho_{\text{snow}}$ ( $\text{kg m}^{-3}$ ) | $R_{\text{opt}}$ (mm) | $T_{\text{soil}}$ (K) | IL | B | Date       |
|------------------------|---------------------------------|---------|-----------------------|---|-----------------------|-----------------------|----|---|------------|
| JB <sub>Feb</sub> -1   | Forest clearing<br>Organic soil | 62      | 266.9 (2.3)           | 240.1 (26.2)                                | 0.21 (0.12)           | 272.8                 | 1  |   | 12-02-2013 |
| JB <sub>Feb</sub> -2   |                                 | 66      | 265.8 (5.0)           | 194.7 (37.8)                                | 0.24 (0.10)           | 273.1                 | 1  |   | 13-02-2013 |
| JB <sub>Feb</sub> -3.1 |                                 | 66      | 265.3 (3.2)           | 250.7 (90.7)                                | 0.18 (0.09)           | 270.8                 | 1  | x | 15-02-2013 |
| JB <sub>Feb</sub> -3.2 |                                 | 66      | 265.6 (3.3)           | 215.9 (57.8)                                | 0.18 (0.09)           | 270.5                 | 1  |   | 15-02-2013 |
| JB <sub>Feb</sub> -3.3 |                                 | 65      | 265.9 (3.0)           | 228.9 (56.5)                                | 0.11 (0.05)           | 270.5                 | 1  |   | 15-02-2013 |
| JB <sub>Feb</sub> -3.4 |                                 | 68      | 266.6 (2.6)           | 228.1 (54.9)                                | 0.17 (0.09)           | 271.3                 | 1  |   | 15-02-2013 |
| JB <sub>Feb</sub> -3.5 |                                 | 65      | 264.0 (4.0)           | 235.4 (66.0)                                | 0.17 (0.10)           | 271.0                 | 1  | x | 15-02-2013 |
| JB <sub>Feb</sub> -3.6 |                                 | 65      | 266.5 (4.7)           | 223.6 (65.8)                                | 0.20 (0.11)           | 271.3                 | 1  |   | 15-02-2013 |
| JB <sub>Feb</sub> -3.7 |                                 | 64      | 266.0 (3.2)           | 209.0 (61.4)                                | 0.18 (0.11)           | 270.8                 | 1  |   | 15-02-2013 |

214  
 215 During the March campaign, five snowpits with a mean  $\rho_{\text{snow}}$  of  $278 \text{ kg m}^{-3}$  and mean  
 216  $R_{\text{opt}}$  of  $0.26 \text{ mm}$  were dug (Table 3). There is a clear increase (70%) of grain size in  
 217 March, linked to a strong temperature gradient metamorphism regime typical of such  
 218 environments. On March 22<sup>nd</sup>, a transect of three snowpits was conducted in a clearing  
 219 with frozen organic soil.

220  
 221 **Table 3.** Same as Table 1, but for James Bay sites in March (JB<sub>Mar</sub>).

| SP                     | Type  | SD (cm) | T <sub>snow</sub> (K) | $\rho_{\text{snow}}$ (kg m <sup>-3</sup> ) | R <sub>opt</sub> (mm) | T <sub>soil</sub> (K) | IL | B | Date       |
|------------------------|---|---------|-----------------------|--|-----------------------|-----------------------|----|---|------------|
| JB <sub>Mar</sub> -1   | Forest clearing<br>Organic soil             | 83      | 268.2 (3.2)           | 261.4 (41.0)                               | 0.25 (0.10)           | 272.0                 | 1  |   | 19-03-2013 |
| JB <sub>Mar</sub> -2   |   | 67      | 267.5 (2.4)           | 265.2 (38.2)                               | 0.25 (0.07)           | 270.9                 | 1  |   | 20-03-2013 |
| JB <sub>Mar</sub> -3.1 | Transect in Forest clearing<br>Organic soil | 63      | 269.3 (0.8)           | 266.1 (34.9)                               | 0.28 (0.11)           | 270.5                 | 1  |   | 22-03-2013 |
| JB <sub>Mar</sub> -3.2 |   | 69      | 271.0 (1.0)           | 303.1 (28.1)                               | 0.26 (0.09)           | 272.5                 | 1  |   | 22-03-2013 |
| JB <sub>Mar</sub> -3.3 |   | 67      | 270.9 (0.8)           | 294.2 (28.1)                               | 0.25 (0.10)           | 272.1                 | 1  |   | 22-03-2013 |

222  
 223 Measurements were also conducted in a forested area (Table 4), where the emission of  
 224 the trees that is reflected on the ground contributes to the measured T<sub>B</sub> (Roy et al., 2012).  
 225 For these reasons, these snowpits were treated separately and used to better understand  
 226 the influence of tree emission on ground-based radiometric measurements. On January  
 227 10<sup>th</sup>, a transect of eight snowpits was conducted in a forested area as well as transects of  
 228 three snowpits on February 14<sup>th</sup> and March 21<sup>st</sup>. In addition to the usual snowpit  
 229 observations, fisheye pictures (Fig. 2) were taken during the January and February  
 230 campaigns to quantify vegetation density. The pictures were binarized to distinguish sky  
 231 pixels from tree pixels allowing the estimation of the proportion of pixels (fraction)  
 232 occupied by vegetation ( $\chi_{\text{veg}}$ ).

233  
 234 **Table 4.** Same as Table 1, but for James Bay sites, all in forested areas (JB<sub>veg</sub>).

| SP                     | Type                   | SD (cm) | T <sub>snow</sub> (K) | $\rho_{\text{snow}}$ (kg m <sup>-3</sup> ) | R <sub>opt</sub> (mm) | T <sub>soil</sub> (K) | IL | Date       |
|------------------------|------------------------|---------|-----------------------|--|-----------------------|-----------------------|----|------------|
| JB <sub>veg</sub> -1   | First transect of 30 m | 62      | 267.6 (1.8)           | 222.5 (44.5)                               | 0.14 (0.08)           | 272.4                 | 1  | 11-01-2013 |
| JB <sub>veg</sub> -2.1 |                        | 64      | 267.4 (2.7)           | 202.6 (43.3)                               | 0.18 (0.09)           | 273.3                 | 1  | 10-01-2013 |
| JB <sub>veg</sub> -2.2 |                        | 67      | 269.0 (2.3)           | 211.6 (49.9)                               | 0.15 (0.09)           | 273.3                 | 1  | 10-01-2013 |
| JB <sub>veg</sub> -2.3 |                        | 60      | 268.3 (3.1)           | 201.4 (58.5)                               | 0.16 (0.09)           | 273.4                 | 1  | 10-01-2013 |
| JB <sub>veg</sub> -2.4 |                        | 60      | 267.6 (2.1)           | 197.2 (40.0)                               | 0.19 (0.10)           | 272.4                 | 1  | 10-01-2013 |
| JB <sub>veg</sub> -2.5 |                        | 65      | 267.1 (2.5)           | 200.7 (48.9)                               | 0.15 (0.08)           | 272.8                 | 1  | 10-01-2013 |
| JB <sub>veg</sub> -2.6 |                        | 60      | 266.3 (2.0)           | 195.5 (59.8)                               | 0.15 (0.08)           | 271.9                 | 1  | 10-01-2013 |
| JB <sub>veg</sub> -2.7 |                        | 56      | 268.4 (2.5)           | 199.4 (36.5)                               | 0.15 (0.09)           | 272.9                 | 1  | 10-01-2013 |
| JB <sub>veg</sub> -2.8 | Second transect of 6 m | 68      | 268.1 (2.9)           | 205.4 (45.2)                               | 0.14 (0.08)           | 273.1                 | 1  | 10-01-2013 |
| JB <sub>veg</sub> -3.1 |                        | 78      | 267.0 (2.8)           | 231.6 (44.1)                               | 0.19 (0.10)           | 272.4                 | 2  | 14-02-2013 |
| JB <sub>veg</sub> -3.2 |                        | 78      | 267.4 (2.4)           | 217.0 (55.8)                               | 0.19 (0.10)           | 272.6                 | 2  | 14-02-2013 |
| JB <sub>veg</sub> -3.3 |                        | 75      | 267.5 (2.2)           | 222.0 (62.1)                               | 0.19 (0.12)           | 272.4                 | 1  | 14-02-2013 |
| JB <sub>veg</sub> -4.1 | Third                  | 88      | 268.1 (1.5)           | 281.4 (55.3)                               | 0.20 (0.11)           | 271.9                 | 3  | 21-03-2013 |

|                        |                    |    |             |              |             |       |   |            |
|------------------------|--------------------|----|-------------|--------------|-------------|-------|---|------------|
| JB <sub>veg</sub> -4.2 | transect<br>of 6 m | 88 | 269.9 (1.5) | 283.2 (42.8) | 0.22 (0.12) | 272.9 | 3 | 21-03-2013 |
| JB <sub>veg</sub> -4.3 |                    | 87 | 271.5 (1.0) | 288.8 (43.7) | 0.28 (0.12) | 272.9 | 3 | 21-03-2013 |

235  
236



237  
238 **Fig. 2.** Fisheye pictures for JBveg-3.3 (left) and JBveg-2.2 (right) sites, showing the sky  
239 view proportion around the SBR site measurements.

240  
241 **2.1.2 Umiujaq**  
242

243 An intensive measurement campaign was conducted in January 2014 (21<sup>st</sup> to 28<sup>th</sup>) in the  
244 region of Umiujaq. All the measurements were conducted in a tundra environment except  
245 for the Umi-3 site, which was located in a clearing (Table 5). The tundra sites were  
246 characterized by typical dense snow drift layers near the surface that fall into the bridging  
247 limits of 0.4 and 0.6 for the ice fraction as defined by Dierking et al. (2012) (see Sect.  
248 2.2.2). Furthermore, one to two ice lenses were observed at the UMI-1, UMI-2 and UMI-  
249 4 sites.  
250

251 **Table 5.** Same as Table 1, but for Umiujaq sites (UMI).

| SP    | Type               | SD<br>(cm) | T <sub>snow</sub> (K) | ρ <sub>snow</sub> (kg m <sup>-3</sup> ) | R <sub>opt</sub> (mm) | T <sub>soil</sub> (K) | IC | B | Date       |
|-------|--------------------|------------|-----------------------|---|-----------------------|-----------------------|----|---|------------|
| UMI-1 | Tundra             | 35         | 253.9 (2.6)           | 361.8 (54.4)                            | 0.15 (0.12)           | 258.4                 | 2  | x | 22-01-2014 |
| UMI-2 |                    | 70         | 256.2 (4.6)           | 379.0 (40.5)                            | 0.18 (0.09)           | 265.2                 | 2  | x | 23-01-2014 |
| UMI-3 | Forest<br>clearing | 132        | 263.5 (5.8)           | 319.0 (51.2)                            | 0.18 (0.08)           | 271.8                 | 0  | x | 24-01-2014 |
| UMI-4 | Tundra             | 57         | 256.9 (4.2)           | 280.7 (46.5)                            | 0.23 (0.11)           | 264.4                 | 1  |   | 25-01-2014 |
| UMI-5 |                    | 93         | 254.0 (3.9)           | 350.6 (42.3)                            | 0.19 (0.09)           | 261.6                 | 0  | x | 26-01-2014 |

252  
253 **2.2 Models**  
254

255 The study uses the DMRT-ML model to simulate the microwave emission of snow-  
256 covered surfaces (Brucker et al. 2011; Picard et al., 2013). It is a multilayer

257 electromagnetic model based on the DMRT theory (Tsang and Kong, 2001). The theory  
258 assumes that a snow layer is composed of ice spheres where the effective permittivity is  
259 calculated using the first-order quasi-crystalline approximation and the Percus-Yevick  
260 approximation. The propagation of energy between the different layers is calculated with  
261 the Discrete Ordinate Radiative transfer (DISORT) method as described in Jin et al.  
262 (1994). In this paper, the propagation of electromagnetic radiation was calculated for 64  
263 streams.

264  
265 The snowpit measurements ( $\rho_{\text{snow}}$ ,  $T_{\text{snow}}$ ,  $T_{\text{soil}}$  and  $R_{\text{opt}}$ ) were integrated as input to the  
266 model to simulate snow microwave emission. However it was shown in previous studies  
267 (Brucker et al. 2011; Roy et al., 2013; Picard et al. 2014) that using  $R_{\text{opt}}$  was inadequate  
268 as input to DMRT-ML. As such, a scaling factor of  $\phi = 3.3$  **assuming non-sticky snow**  
269 **grains** from Roy et al. (2013) for the seasonal snowpack is thus applied to get an effective  
270 radius in the microwave range ( $R_{\text{eff}}$ ):  
271

$$272 \quad R_{\text{eff}} = R_{\text{opt}} \cdot \phi \quad (2)$$

273 Roy et al. (2013) shows that the need for a scaling factor in DMRT-ML could be related  
274 to the grain size distribution of snow and the stickiness between grains, which leads to an  
275 increase of the  $R_{\text{eff}}$ .  
276

277 The atmospheric downwelling  $T_B$  that is reflected by the snow surface to the radiometer  
278 was modeled using the millimeter-wave propagation model (Liebe et al., 1989)  
279 implemented in the Helsinki University of Technology (HUT) snow emission model  
280 (Pulliajainen et al., 1999). The atmospheric model was driven with the air temperature and  
281 air moisture of the atmospheric layer above the surface from the 29 North American  
282 Regional Reanalysis (Mesinger et al., 2006) atmospheric layers.  
283

### 284 2.2.1 Ice lenses

285 The microwave signal is very sensitive to ice lens formation within a snowpack at H-pol  
286 (Montpetit et al., 2013; Rees et al., 2010; Lemmetyinen et al., 2010). To simulate the ice  
287 lenses present in this study's database (see Tables 1 to 5) using DMRT-ML, snow layers  
288 with a high density of  $900 \text{ kg m}^{-3}$  close to the density of pure ice ( $917 \text{ kg m}^{-3}$ ) and a null  
289 snow grain size were integrated into the snowpack input file where ice lenses were  
290 observed. The value of  $900 \text{ kg m}^{-3}$  was chosen because only pure ice lenses were  
291 observed. **To keep the same total snow depth, the adjoining layers were adjusted by**  
292 **removing 0.5 cm of the layer above and below the ice layer.** However, an analysis of the  
293 effect of ice lens density on  $T_B$  simulations will be conducted in Sect. 3.2.4. Because  
294 coherence is neglected in DMRT-ML (Matzler, 1987), the ice lens thickness has a  
295 negligible effect on simulated  $T_B$ . Hence, because no precise measurements of ice lens  
296 thickness were performed in the field, ice lens thickness was set to 1 cm in DMRT-ML.  
297

298

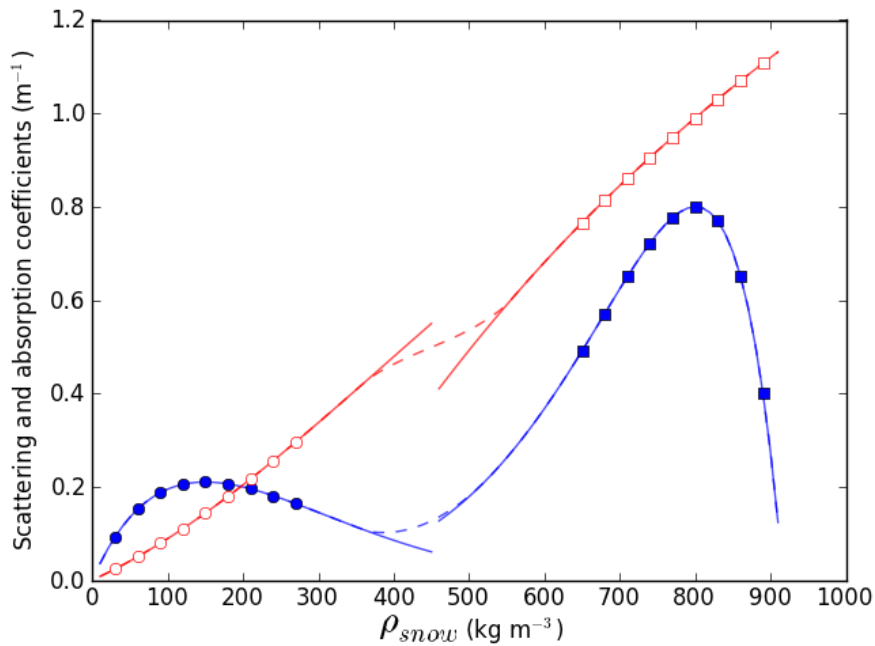
300

301 **2.2.2 Bridging**

302

303 It has been shown that DMRT theory is in agreement with numerical solutions of the 3-D  
 304 Maxwell equations up to a density of  $275 \text{ kg m}^{-3}$  (ice fraction of 0 - 0.3) (Tsang et al.,  
 305 2008), which is a relatively low density for snow. Although most of the applications of  
 306 DMRT theory concern snow, DMRT can be applied to other dense media such as bubbly  
 307 ice (Dupont et al., 2014). In this case, the background is pure ice, and the scatterers are  
 308 air spheres to represent bubbles. To the best of our knowledge, no validity tests have been  
 309 done in this configuration; but if we assume a similar range of validity in terms of volume  
 310 fraction of scatterers, the DMRT theory would be valid in the range 0.7 – 1 for the ice  
 311 fraction, that is  $642 - 917 \text{ kg m}^{-3}$ . Even in this case, a large range of intermediate densities  
 312 remains for which the absorption and scattering coefficients might not be accurate.  
 313 Following Dierking et al. (2012), an empirical extrapolation of these coefficients from a  
 314 spline fitted in both validity ranges was implemented to calculate coefficients for a layer  
 315 with an ice fraction between 0.4 ( $\rho_{\text{snow}} = 367 \text{ kg m}^{-3}$ ) and 0.6 ( $\rho_{\text{snow}} = 550 \text{ kg m}^{-3}$ ) (Fig. 3).  
 316 As an example, the bridging leads to a decrease of  $T_B$  at 37 GHz for high snow density ( $> 350 \text{ kg m}^{-3}$ ) related to the increase of scattering (Fig. 4). In the following, this approach is  
 317 denoted as ‘bridging’ and the limits will be set at 0.4 and 0.6 for the ice fraction  
 318 following the study of Dierking et al. (2012).  
 319

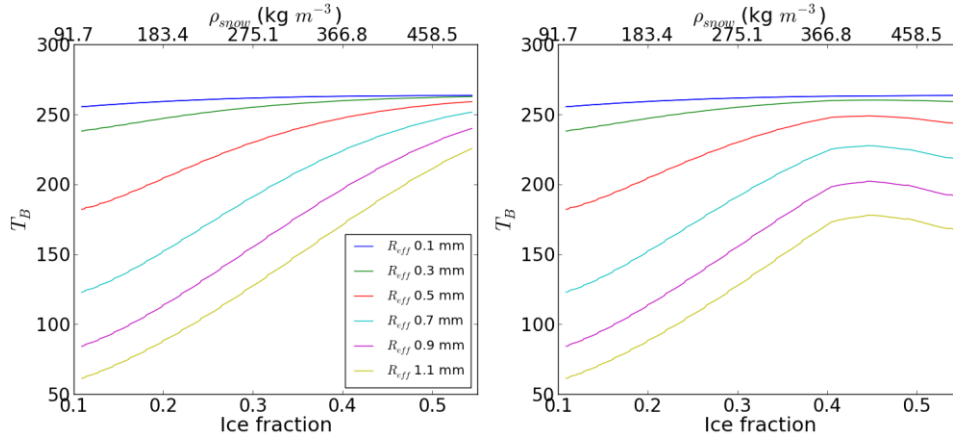
320



321

322 **Fig. 3.** Absorption (red) and scattering (blue) coefficients as a function of  $\rho_{\text{snow}}$  at 37 GHz  
 323 ( $T_{\text{snow}} = 260 \text{ K}$ ,  $T_{\text{soil}} = 270 \text{ K}$ ,  $SD = 1.0 \text{ m}$  and  $R_{\text{eff}} = 0.3 \text{ mm}$ ). The dotted lines show the  
 324 bridging implementation for an ice fraction between 0.4 and 0.6.

325



326

327 **Fig. 4.**  $T_B$  without (left) and with the bridging implementation (right) at 37 GHz (V-pol)  
328 for different  $R_{eff}$  ( $T_{snow} = 260$  K,  $T_{soil} = 270$  K and SD = 1.0 m).

329

330 The implementation of the bridging was evaluated with James Bay and Umiujaq snowpit  
331 data that include at least one snow layer with an ice fraction of more than 0.4 (Tables 2  
332 and 5). Because  $\rho_{snow}$  is relatively low in boreal regions due to weakening of the wind by  
333 trees, we also evaluated this approximation using a tundra dataset to increase the number  
334 of high density snow layers for the specific validation of the bridging. The database  
335 acquired at the Churchill Northern Studies Center (58°44'N, 93°49'W) (Roy et al., 2013;  
336 Derksen et al., 2012) from the winter 2010 campaign is composed of 13 sites with at least  
337 one layer in the bridging range.

338

### 339 2.2.3 Soil model

340

341 Soil reflectivity models are included in DMRT-ML to account for the soil contribution to  
342 the measured  $T_B$ . In this paper, the Wegmüller and Mätzler (1999) soil reflectivity model  
343 improved for frozen soil by Montpetit et al. (2015) is used. The Wegmüller and Mätzler  
344 (1999) model for incidence angles lower than 60° is described by:

$$345 \quad \Gamma_{f,H-pol} = \Gamma_{f,H}^{Fresnel} \exp(-(k\sigma)^{\sqrt{-0.1\cos\theta}}) \quad (3)$$

346

$$347 \quad \Gamma_{f,V-pol} = \Gamma_{f,H} \cos\theta^\beta \quad (4)$$

348

349 where  $\Gamma_{f,p}$  is the rough soil reflectivity at a frequency  $f$  and polarization  $p$  (H-pol or V-  
350 pol) by its smooth Fresnel reflectivity in H-Pol ( $\Gamma_{f,H}$ ), which depends on the incidence  
351 angle ( $\theta$ ) and the real part of the soil permittivity ( $\epsilon'$ ), weighted by an attenuation factor  
352 that depends on the standard deviation in height of the surface (soil roughness,  $\sigma$ ), the  
353 measured wavenumber ( $k$ ) and a polarization ratio dependency factor ( $\beta$ ). The values of  
354  $\epsilon'$ ,  $\sigma$  and  $\beta$  at 11, 19 and 37 GHz inverted by Montpetit et al. (2015) for frozen soil (Table

355 6) were used in this study. Montpetit et al. (2013) used independent snow free ground-  
356 based radiometer angular measurements taken at James Bay site in 2013 (same  
357 campaign). The parameters were also validated over Umiujaq (same campaign) from  
358 snow removal experiment.

359 **Table 6.** Main parameters used in DMRT-ML

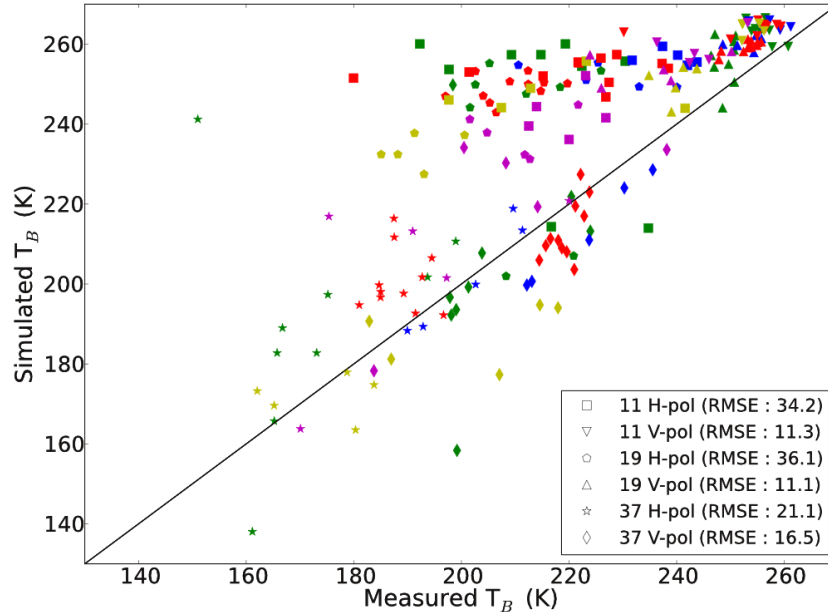
| Frequency (GHz) | $\epsilon$ | $\beta$ | $\phi$ | fluxes | $\sigma$ (cm) | $\theta$ ( $^{\circ}$ ) |
|-----------------|------------|---------|--------|--------|---------------|-------------------------|
| 11              | 3.197      | 1.077   | 3.3    | 64     | 0.193         | 55                      |
| 19              | 3.452      | 0.721   |        |        |               |                         |
| 37              | 4.531      | 0.452   |        |        |               |                         |

361 **3. Results**

362 In this section, the impact of model improvements (ice lenses and bridging) is first  
363 presented. Afterward, the evaluation of the effect of the different sources (soil, snow  
364 grain size, snow density, ice lenses and vegetation) on  $T_B$  is shown.

365 **3.1 Model validation and improvement**

366 Initial simulations ignoring the presence of ice lenses and bridging show a clear  
367 overestimation of  $T_B$  mostly at H-pol. The observed root mean square error (RMSE) is  
368 greater than 35 K at 11 and 19 GHz and greater than 20 K at 37 GHz (Fig. 5). There is  
369 also a positive bias for  $T_B$  at 11 and 19 GHz at V-pol. In this section, the effect of ice  
370 lenses on  $T_B$  is evaluated, while the bridging implementation was tested on snowpits data.  
371

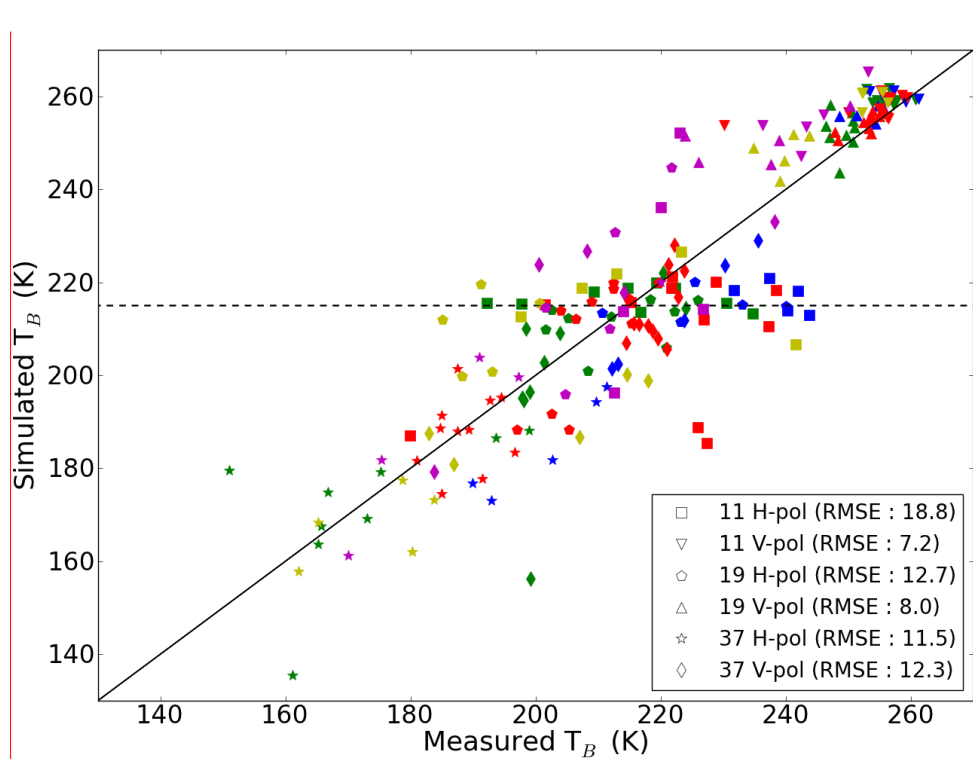


376  
 377 **Fig. 5.**  $T_B$  simulated without ice lenses in DMRT-ML and bridging. RMSE (K) between  
 378 measured and simulated  $T_B$  are given in parentheses. The symbol types correspond to the  
 379 frequency and colors to the sites: Red = JB<sub>Jan-transect</sub>; Green = JB<sub>Jan-others</sub>; Blue = JB<sub>Feb</sub>;  
 380 Yellow = JB<sub>Mar</sub>; Magenta = UMI.

381 **3.1.1 Ice lenses**

384 Simulations including observed ice lenses were conducted on all snowpits (Fig. 6)  
 385 leading to a strong decrease in simulated  $T_B$  H-pol (up to 40 K). At H-pol, the RMSE are  
 386 thus improved by 15.4, 23.4 and 9.3 K at 11, 19 (initially  $> 35$  K) and 37 GHz (initially  $>$   
 387 20 K) respectively. The ice lenses also slightly decrease the bias measured at V-pol for all  
 388 frequencies leading to a RMSE improvement of 3 to 4 K. These results show that a  
 389 simple ice lens implementation in DMRT-ML helps to simulate the strong reflection  
 390 component of ice lenses (decrease of snowpack emissivity), leading to improved  
 391 simulations of  $T_B$ .

392 However, a large variability (190 to 245 K) in  $T_B$  observations at H-pol at 11 and 19 GHz  
 393 is not reproduced by the simulations (dotted black line in Fig. 6). This feature suggests  
 394 some limitations of ice lens and/or snow layering modeling in DMRT-ML that can be  
 395 related to the fact that coherence effect is not taken into account. Note that this  
 396 underestimation of  $T_B$  spatial variability is not related to the soil as it is demonstrated in  
 397 Sect. 3.2.1. The modeling uncertainties related to ice lenses will be discussed more  
 398 specifically in Sect. 3.2.4.



Comment [AR2]: The dotted line was added

402  
403 **Fig. 6.**  $T_B$  simulated with ice lenses included in DMRT-ML, but without bridging. The  
404 symbol types correspond to the frequency and colors to the sites: Red = JB<sub>Jan-transect</sub>,  
405 Green = JB<sub>Jan-others</sub>; Blue = JB<sub>Feb</sub>; Yellow = JB<sub>Mar</sub>; Magenta = UMI. The dotted black line  
406 represents the  $T_B$  where the simulations underestimated the spatial variability at 11 and  
407 19 GHz H-pol.

### 408 3.1.2 Bridging

411 To test the bridging parameterization (see Sect 2.2.2), we used 13 tundra sites from the  
412 Churchill tundra database (Roy et al., 2013), 4 from Umiujaq and 2 from the James Bay  
413 snowpits. In each case, at least one snow layer with a snow density higher than  $367 \text{ kg m}^{-3}$   
414 (ice fraction of 0.4; Dierking et al., 2012) is used. For each of the 19 sites studied,  
415 simulations at 37 GHz (the most sensitive frequency to snow) with and without the  
416 bridging implementation were conducted (all input parameters kept the same). The  
417 bridging has a relatively modest impact on simulations with an improvement in the  
418 RMSE of between 2 and 4 K at tundra sites (Umiujaq and James Bay). The greatest  
419 improvements are found for deep drifted tundra snowpits where there is a very thick wind  
420 slab with high  $\rho_{\text{snow}}$  and small rounded grains are present at the top of the snowpack.

Comment [AR3]: The old Fig. 6 was removed (bridging scatterplot)

### 422 3.2 Signal contributions and modeling uncertainties

424 In the following, all DMRT-ML simulations consider the bridging implementation and  
 425 include the observed ice lenses. Table 7 shows the overall RMSE for all campaigns that  
 426 are described in Sect. 3.3.1 to 3.3.4. The RMSE values oscillate between 7.8 and 21.5 K  
 427 at H-pol (Table 7). Since V-pol is less affected by layering in the snowpack at 11 GHz  
 428 and 19 GHz, the RMSE are generally lower (between 3.5 and 14.4 K), while the RMSE  
 429 at 37 GHz are similar at V-pol and H-pol. This is due to the higher sensitivity of higher  
 430 frequencies to snow grain scattering when compared to the lower frequencies that are less  
 431 affected by stratigraphy. Table 7 also suggests that the inclusion of bridging only  
 432 decreases the RMSE by 0.5 K and 0.3 K at 37 GHz at H-pol and V-pol respectively (see  
 433 Fig. 5). These RMSE will thus be used as a reference to quantify the effect of spatial  
 434 variability and uncertainty in measurements on the  $T_B$  simulations.

435  
 436 **Table 7:** Overall RMSE (K) between measured and simulated  $T_B$  for all sites considering  
 437 ice lenses and bridging in DMRT-ML.

|     | JB <sub>Jan</sub> | JB <sub>Feb</sub> | JB <sub>Mar</sub> | UMI  | All  |
|-----|-------------------|-------------------|-------------------|------|------|
| 11H | 21.5              | 13.6              | 18.2              | 14.3 | 18.8 |
| 11V | 6.4               | 5.5               | 6.3               | 9.8  | 7.2  |
| 19H | 11.7              | 8.7               | 19.8              | 11.2 | 12.7 |
| 19V | 3.5               | 5.7               | 9.2               | 13.4 | 8.0  |
| 37H | 12.1              | 15.1              | 9.7               | 9.7  | 11.5 |
| 37V | 7.8               | 15.3              | 14.4              | 16.8 | 12.3 |

### 438 439 3.2.1 Soil roughness

440 The analysis of small-scale soil variability in modeling the  $T_B$  of snow-covered surfaces  
 441 is conducted using the SEex from the transect during the JB<sub>Jan</sub> (mineral soil) and JB<sub>Feb</sub>  
 442 campaigns (organic soil). The JB<sub>Jan</sub> SEex data represent the variability within a 30 m  
 443 transect in a relatively homogeneous mineral soil area (quarry). The JB<sub>Feb</sub> SEex were  
 444 conducted at four different locations in clearings with organic soil and within about 1 km  
 445 from each other. The strategy behind the evaluation of the small-scale spatial variability  
 446 on snow-covered  $T_B$  is to first calculate the soil emission variability (optimization of  $\sigma$ )  
 447 from SEex measurements. This variability is then introduced in the simulations with  
 448 snow-covered surfaces to evaluate the sensitivity of  $T_B$  to variability in the emission of  
 449 frozen soil.

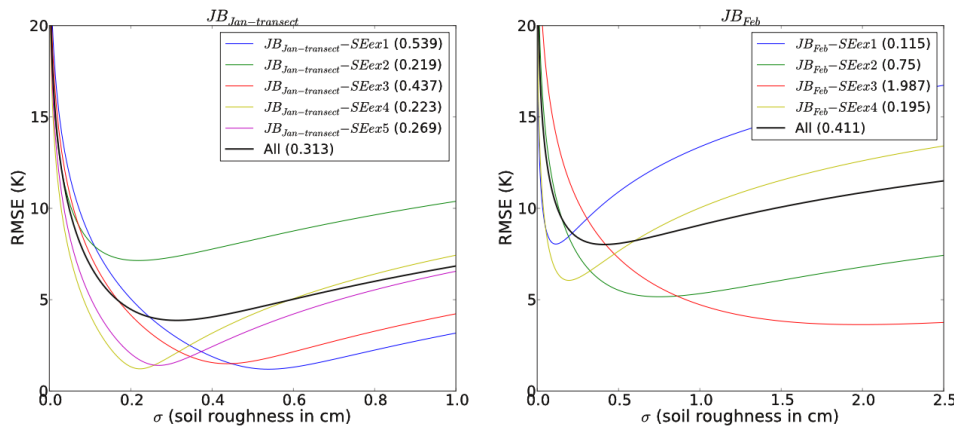
450 For each SEex measurement, the surface roughness parameter  $\sigma$  was optimized using the  
 451 three frequencies and both polarizations for bare soil measurements. The  $\sigma$  value was  
 452 changed by increments of 0.01 cm, up to 1 cm (Eq. 3 and 4) and the associated RMSE $_{\sigma}$   
 453 was calculated as a function of the measured  $T_B$  ( $T_{B\text{mes}}$ ) and simulated  $T_B$  ( $T_{B\text{sim}}$ ) in V-pol  
 454 and H-pol as follows:

$$455 \quad RMSE_{\sigma} = \sqrt{\frac{\sum_{j=1}^3 \sum_{i=1}^N (T_{B\text{sim};i}^{jV} - T_{B\text{mes};i}^{jV})^2 + (T_{B\text{sim};i}^{jH} - T_{B\text{mes};i}^{jH})^2}{6N}} \quad (5)$$

460  
 461 where  $j$  corresponds to the frequencies ( $j=1,2,3$  respectively for 11, 19 and 37 GHz) and  $i$   
 462 corresponds to the sites. The optimal  $\sigma$  was determined by the lowest  $\text{RMSE}_\sigma$  (Eq. 5)  
 463 value for all sites at  $\text{JB}_{\text{Jan}}$  and  $\text{JB}_{\text{Feb}}$ .  
 464

465 The optimization was also done for each site individually to estimate the spatial  
 466 variability in  $\sigma$ . The results presented in Fig. 7 show that a clear minimum in the  $\text{RMSE}_\sigma$   
 467 can be found at every site. Fig 7 (right) shows that the optimal  $\sigma$  at  $\text{JB}_{\text{Jan-transect}}$  values are  
 468 located between 0.22 and 0.54 cm, while 0.31 is found for all 5 sites. The variability can  
 469 be explained by the variation of the gravel size that affects the surface roughness. For  
 470  $\text{JB}_{\text{Feb}}$ , the observed spatial variability is more significant with variations ranging between  
 471 0.195 cm and 1.987 cm with an optimized  $\sigma = 0.411$  cm for all 4 sites (Fig. 7 left).  
 472 **However, one should be careful in interpreting these results as the optimization could**  
 473 **also compensate for uncertainties in the permittivity of frozen ground. Nevertheless,**  
 474 **because the minimal and maximal values of optimized  $\sigma$  are taken, this does not affect**  
 475 **our main goal, which is to estimate the variability in snow-covered  $T_B$  introduced by the**  
 476 **soil in the model. Furthermore, as mentioned in Sect. 2.2.3, the permittivity used in this**  
 477 **study were retrieved at the same site as this study.**

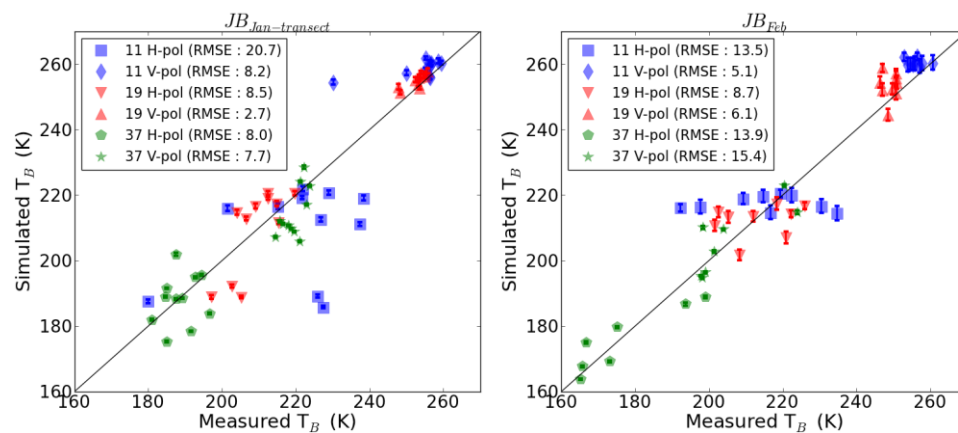
478



479  
 480 **Fig. 7.**  $\text{RMSE}_\sigma$  for bare frozen soil sites (snow excavation experiment, SEEx) as a  
 481 function of soil roughness ( $\sigma$ ) for (left)  $\text{JB}_{\text{Jan-transect}}$  and (right)  $\text{JB}_{\text{Feb}}$ . The optimized  $\sigma$  for  
 482 each site is given in parentheses.  
 483

484 We evaluated the small-scale spatial variability of soil emissivity resulting from the  
 485 observed roughness variability. For the sites with observations taken with snow on the  
 486 ground (Tables 1, 2, 3 and 5, for both campaigns), we simulated the  $T_B$  with DMRT-ML  
 487 considering the lowest and highest optimized  $\sigma$  (see Fig. 7). Note that we have not used  
 488 the standard deviation of  $\sigma$  that would have led to negative values. Fig. 8 (left) shows that  
 489 the  $T_B$  sensitivity to the variation of soil roughness is very weak.  $T_B$  variations of 0.5 K  
 490 and 1.3 K were observed at the  $\text{JB}_{\text{Jan-transect}}$  site where the soil properties were more  
 491 homogeneous (**mineral soil**), while a variation of 0.7 K to 3.8 K was measured at the  
 492  $\text{JB}_{\text{Feb}}$  site with **organic soil** (Table 8). The sensitivity is higher at 11 and 19 GHz because  
 493 the soil emission is less attenuated by snow grain scattering. We also performed the same

494 calculation without the ice lens implementation where results are similar (less than 1 K  
 495 change) suggesting that despite a potential low transmissivity, ice lenses are not  
 496 responsible for the attenuation of the soil upwelling emission.  
 497



498  
 499 **Fig. 8.** Sensitivity of snow-covered surface  $T_B$  to the variation of soil roughness ( $\sigma$ ) for  
 500 (left)  $JB_{Jan\text{-transect}}$  and (right)  $JB_{Feb}$ . The error bars show the variation of  $T_B$  for maximum  
 501 and minimum optimized  $\sigma$  derived from SEx during both campaign (Fig. 7). The RMSE  
 502 (K) values correspond to the retrievals using the initial (Table 6)  $\sigma$  value.  
 503

504 **Table 8:**  $T_B$  sensitivity ( $\Delta T_B$ ) (K) associated with the small-scale variability of soil  
 505 roughness ( $\sigma$ ).

|     | $JB_{Jan\text{-transect}}$ | $JB_{Feb}$ |
|-----|----------------------------|------------|
| 11H | 1.3                        | 3.8        |
| 11V | 1.3                        | 3.8        |
| 19H | 1.2                        | 3.2        |
| 19V | 1.4                        | 3.5        |
| 37H | 0.5                        | 0.7        |
| 37V | 0.6                        | 0.7        |

506 The results show that the soil small-scale spatial variability is much lower than the RMSE  
 507 for most of the frequencies and polarizations (Tables 7 and 8). However, for 11 and 19  
 508 GHz at V-pol, the soil-induced variability calculated during  $JB_{Feb}$  campaign leads to  $\Delta T_B$   
 509 values (Table 8) similar to the measured RMSE (Table 7). Hence, the modeling error  
 510 cannot be solely explained by small-scale variability in the emissivity of frozen soil,  
 511 except possibly for 11 and 19 GHz at V-pol. However, these conclusions are only valid  
 512 for frozen soils, but the higher dielectric contrast of thawed soil would have a greater  
 513 impact on the emissivity of snow-covered surfaces.  
 514

### 3.2.2 Snow grain size

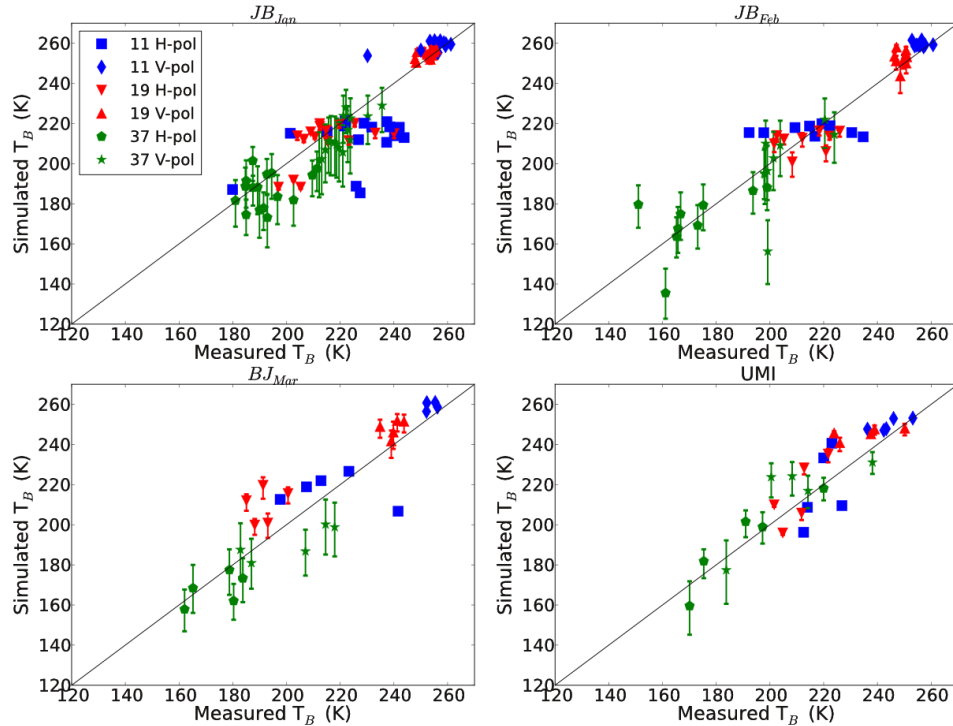
515 To test the sensitivity of the simulations to the grain size (SSA) measurement errors, the  
 516 simulations considered an error of 12% in SSA when using the shortwave infrared  
 517 reflection measurement approach as reported in Gallet et al. (2009). Hence two  
 518 simulations were conducted: one with all SSA data along the profile increased by 12%

522 ( $T_{BSSA+12\%}$ ), and one with all SSA data decreased by 12% ( $T_{BSSA-12\%}$ ). From these two  
523 simulations, the variation of  $T_B$  related to SSA errors ( $\Delta T_{BSSA}$ :  $T_{BSSA+12\%} - T_{BSSA-12\%}$ ) was  
524 calculated, keeping in mind that this should be the maximum  $\Delta T_B$  error, since the  
525 variations in SSA are all in the same direction for the whole profile. The soil  
526 parameterization is kept the same for all sites (see Table 6).

527  
528 Figure 9 shows the error bars related to a variation of + 12% in SSA (upper bars: higher  
529 SSA leads to smaller grains and less scattering) and - 12 % (lower bars: lower SSA leads  
530 to larger grains and more scattering). The results show that 37 GHz is the most sensitive  
531 to the grain size with variations between 16.2 K and 27.4 K (Table 9). The variations are  
532 generally higher at V-pol, which has a higher penetration depth with less sensitivity to  
533 stratification and ice lenses. As such, 37 GHz is more influenced by large depth hoar  
534 grains at the bottom of the snowpack. Hence, because the relationship between the  
535 scattering and the particle size reaches a maximum sensitivity within the particle range  
536 (Picard et al. 2013), the variation of 12% for depth hoar SSA will cause a higher increase  
537 of  $\Delta T_{BSSA}$ . In all cases,  $\Delta T_{BSSA}$  are higher than the RMSE (Table 7) suggesting that grain  
538 size can explain the uncertainty in the  $T_B$  simulations.

539  
540 At 19 GHz, there is an increase in  $\Delta T_{BSSA}$  of about 7 K at V-pol and H-pol during the  
541 three James Bay campaigns. This increase of  $\Delta T_{BSSA}$  is linked to snow grain  
542 metamorphism (Colbeck, 1983) that tends to increase the particle size through the winter  
543 (see Table 1, 2 and 3). With a higher sensitivity on the particle range and the dependence  
544 of scattering to the particle size, the variation of large grains will increase  $\Delta T_{BSSA}$ . This  
545 phenomenon shows that at 19 GHz, the effect of SSA measurement uncertainty on  $T_B$   
546 depends on the type of grains. For small snow grains in January, the error in SSA is small  
547 compared to the RMSE, which is not the case in March where the error is closest to the  
548 RMSE in the presence of larger grains. A very small increase of  $\Delta T_{BSSA}$  is also seen at 11  
549 GHz, but with much lower  $\Delta T_{BSSA}$  (less than 1 K). These results show that scattering is  
550 negligible at 11 GHz for seasonal snow, even with large grains such as depth hoar.

551  
552 We assessed average variation in  $T_B$  resulting from 100 runs with random error between  
553  $\pm 12\%$  applied to SSA for each layer and snowpit. As expected, the results show that the  
554 variations between initial simulation and simulation with random error on SSA are  
555 significantly lower than those shown in Table 9. With random error applied on SSA  
556 measurements, the variations are lower than 1 K at 11 and 19 GHz, and between 2 and 3  
557 K at 37 GHz. These values give the lower limits of  $T_B$  error related to SSA uncertainties,  
558 while values in Table 9 give the highest limit of the variation in  $T_B$ .



560  
561 **Fig. 9.**  $T_B$  sensitivity associated to the error of SSA measurements (12%) for the James  
562 Bay (three dates) and Umiujaq sites.  
563

564 **Table 9:**  $T_B$  sensitivity ( $\Delta T_{BSSA}$ :  $T_{BSSA+12\%} - T_{BSSA-12\%}$ ) (K) associated with the error of  
565 SSA measurements

|     | JB <sub>Jan</sub> | JB <sub>Feb</sub> | JB <sub>Mar</sub> | UMI  |
|-----|-------------------|-------------------|-------------------|------|
| 11H | 0.3               | 0.7               | 1                 | 0.5  |
| 11V | 0.3               | 0.7               | 1.1               | 0.5  |
| 19H | 2.8               | 6.5               | 10                | 4.5  |
| 19V | 3.3               | 6.9               | 11.1              | 4.5  |
| 37H | 21.2              | 21.6              | 22.5              | 16.2 |
| 37V | 27.4              | 26.7              | 25.9              | 18.6 |

### 566 3.2.3 Snow density

567 A similar analysis was conducted to evaluate the  $T_B$  sensitivity to an error in  $\rho_{\text{snow}}$  of +/-  
568 10% ( $T_B\rho_{\text{snow}+10\%}$  and  $T_B\rho_{\text{snow}-10\%}$ ). The ice lens density was left at  $900 \text{ kg m}^{-3}$  and the  
569 variations in  $T_B$  related to the  $\rho_{\text{snow}}$  error ( $\Delta T_B\rho_{\text{snow}}$ :  $T_B\rho_{\text{snow}+10\%} - T_B\rho_{\text{snow}-10\%}$ ) were  
570 calculated.

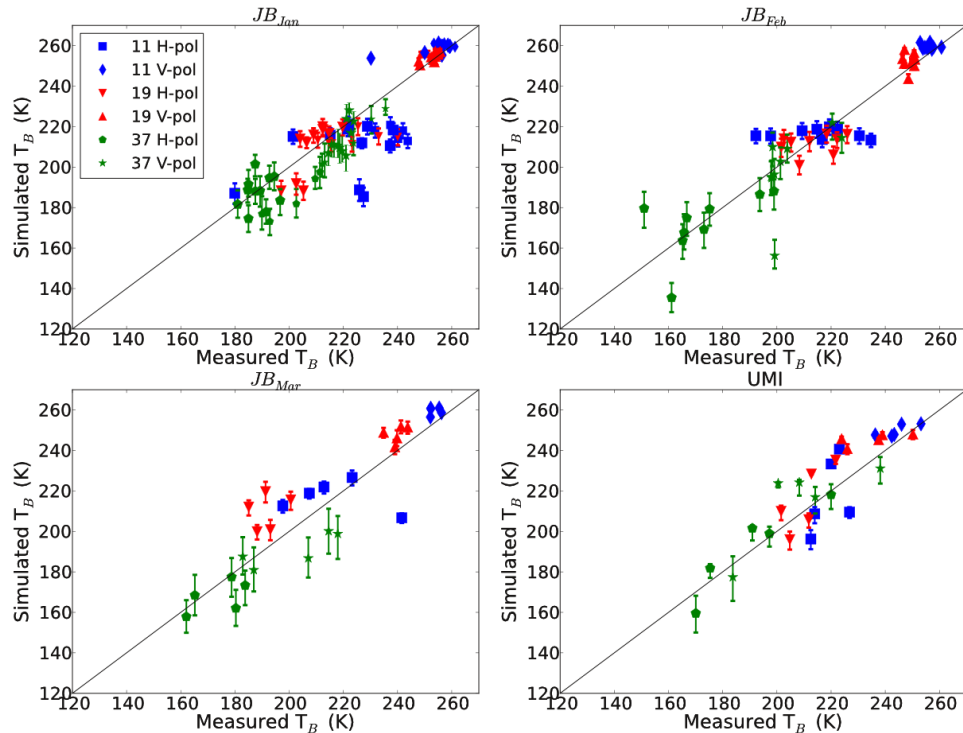
571 The highest sensitivity to  $\rho_{\text{snow}}$  is seen at 37 GHz (Fig. 10). The  $\Delta T_B\rho_{\text{snow}}$  are about 13 K  
572 during the JB<sub>Jan</sub> campaign and increase to 20 K for JB<sub>Mar</sub> (Table 10). Again, this increase  
573 is explained by the growth in snow grain size due to snow metamorphism that leads to  
574 lower density values. In the given range of sphere sizes and  $\rho_{\text{snow}}$  at 37 GHz, the impact

578 of  $\rho_{\text{snow}}$  on  $T_B$  increases with a larger grain size (Fig. 3). These results show that the effect  
 579 of  $\rho_{\text{snow}}$  at 37 GHz on DMRT-ML simulations depends on grain size and evolves  
 580 throughout the winter due to snow metamorphism. It should, however, be noted that if the  
 581 ice fraction limits of the bridging (Sect. 3.1.2) were extended to a lower ice fraction  
 582 density, the impact for high  $\rho_{\text{snow}}$  would be lower or even the opposite, because of the  
 583 increase in scattering due to bridging. Table 10 shows that  $\Delta T_B \rho_{\text{snow}}$  are of the same  
 584 magnitude as RMSE. Hence, depending on the grain size,  $\rho_{\text{snow}}$  can explain part of the  
 585 error in the simulations.

586

587 At 11 and 19 GHz, the highest  $\Delta T_B \rho_{\text{snow}}$  are found at H-pol with values around 7 K  
 588 (Table 10). These highest values are related to the change in the permittivity discontinuity  
 589 between layers, mostly at interfaces around the ice lenses leading to a change in the  
 590 reflectivity at the different interfaces (Montpetit et al., 2013). Because V-pol is less  
 591 affected by horizontal layering, the effect is smaller. Hence, the effect of  $\rho_{\text{snow}}$  uncertainty  
 592 on  $T_B$  is lower than the measured RMSE at 11 and 19 GHz, but has a significant impact  
 593 on  $T_B$  at H-pol. These results are in agreement with studies that show that the microwave  
 594 polarization ratio (H-pol/V-pol) can potentially be used for snow density retrievals  
 595 (Champollion et al., 2013; Lemmettyinen et al., submitted).

596



597

598 **Fig. 10.**  $T_B$  sensitivity associated with the error in snow density measurements ( $\pm 10\%$ ).  
 599 The ice lens density remains at  $900 \text{ kg m}^{-3}$ .

600

601 **Table 10.**  $T_B$  sensitivity ( $\Delta T_B \rho_{\text{snow}}$ :  $T_B \rho_{\text{snow}+10\%} - T_B \rho_{\text{snow}-10\%}$ ) (K) associated with the error  
 602 in snow density measurements

|     | JB <sub>Jan</sub> | JB <sub>Feb</sub> | JB <sub>Mar</sub> | UMI  |
|-----|-------------------|-------------------|-------------------|------|
| 11H | 7.6               | 7.5               | 5.6               | 6.1  |
| 11V | 1.4               | 1.4               | 2.1               | 1.9  |
| 19H | 8                 | 8.8               | 8.3               | 6.2  |
| 19V | 2.4               | 3.2               | 6.7               | 3.6  |
| 37H | 13.5              | 16.5              | 18.4              | 11.6 |
| 37V | 12.6              | 15.3              | 21.4              | 13.4 |

603

604

### 605 3.2.4 Ice lenses

606

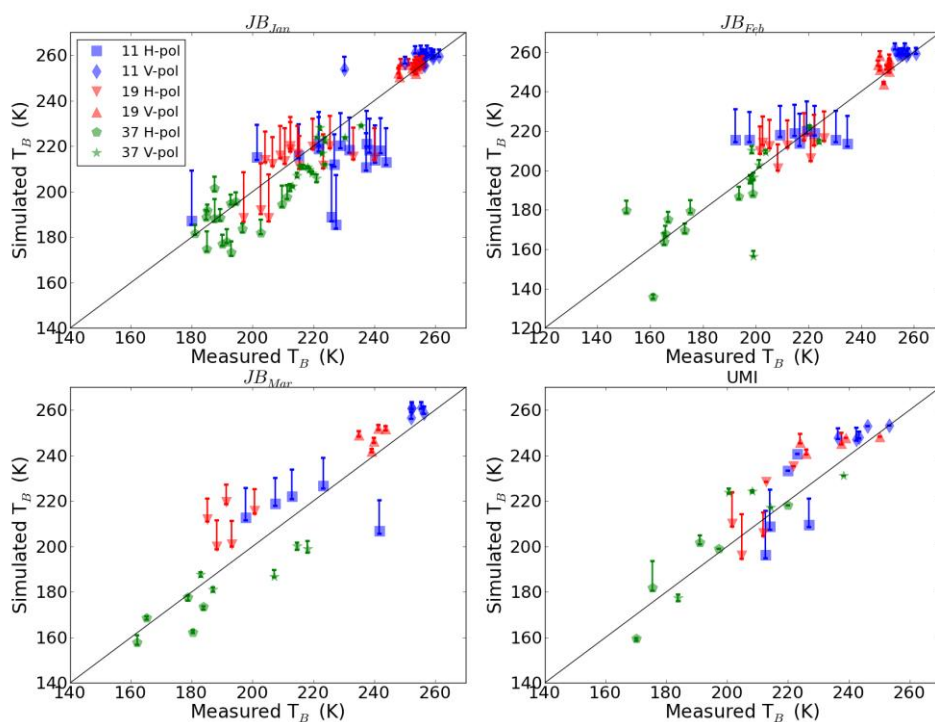
607 While including ice lenses in DMRT-ML significantly reduces the RMSE (section 3.1.1),  
 608 the underestimation of  $T_B$  variability remains strong at 11 and 19 GHz. Given that the  
 609 remaining bias cannot be explained by the soil, grain size or  $\rho_{\text{snow}}$  (Sect. 3.3.1, 3.3.2 and  
 610 3.3.3), we further explore here the role of ice lenses. The ice lens density ( $\rho_{\text{IL}}$ ) variations  
 611 can explain part of the variability as the density of ice influences the internal reflection  
 612 (Durand et al., 2008; Rutter et al., 2013). In fact, ice lenses can be snow crusts with a  
 613 density as low as  $630 \text{ kg m}^{-3}$  (Marsh and Woo, 1984). However, measuring the density of  
 614 such layers is challenging and it was not attempted during our campaigns. The sensitivity  
 615 was evaluated for a range of ice density between  $700 \text{ kg m}^{-3}$  ( $T_B \rho_{\text{IL}700}$ ) and  $917 \text{ kg m}^{-3}$   
 616 ( $T_B \rho_{\text{IL}917}$ ) for all snowpits with ice lenses. The variation of  $T_B$  related to  $\rho_{\text{IL}}$  uncertainties  
 617 ( $\Delta T_B \rho_{\text{IL}}$ :  $T_B \rho_{\text{IL}917} - T_B \rho_{\text{IL}700}$ ) was then calculated (all other parameters being constant).

618

619 Figure 11 shows that  $\rho_{\text{IL}}$  variations have a significant impact on H-pol  $T_B$  mostly at 11  
 620 and 19 GHz. The low  $\Delta T_B \rho_{\text{IL}}$  at 37 GHz (Table 11) is not related to the insensitivity of 37  
 621 GHz to ice lenses, but rather to the attenuation owing to snow grains dominating the  
 622 effect of ice lenses. In fact, Table 11 shows that the effect of the variation of ice lens  
 623 density decreases throughout the winter at James Bay because of increasing attenuation  
 624 related to grain size metamorphism. It should be noted that no scattering occurs in these  
 625 layers in the model because the  $R_{\text{eff}}$  was kept null. Hence,  $\rho_{\text{IL}}$  can only explain the  
 626 underestimation of  $T_B$ , not the overestimation. Part of the error could be explained by the  
 627 coherence that is not taken into account in DMRT-ML. The coherence is caused by  
 628 multiple reflections within a thin layer and associated interference when the thickness of  
 629 the ice lenses is less than a quarter of the wavelength ( $\lambda/4$ ) (Mätzler et al., 1987;  
 630 Montpetit et al., 2013). Since DMRT-ML does not take into account the coherence, the  
 631 thickness of the ice layer has a negligible impact on  $T_B$  and was kept at 1 cm. However,  
 632 simulations with MEMLS accounting for coherence have shown that variation in the ice  
 633 lens thickness can change  $T_B$  by up to 100 K at H-pol at 19 and 37 GHz (Montpetit et al.,  
 634 2013). Also, in this study, only the main ice lenses were noted and inserted in DMRT-  
 635 ML. Many other melt/refreeze thin snow crusts were present but not recorded, and they  
 636 can have a large impact on  $T_B$  observations (see Rutter et al., 2013). These thin crusts  
 637 (less than 2 mm) with a high density (over  $600 \text{ kg m}^{-3}$ ) can also have significant  
 638 coherence effects (less than  $\lambda/4$ ).

639

640 During the JB<sub>Jan</sub> campaign, at the transect, two ice lenses were observed at three  
 641 consecutive snowpits (JB<sub>Jan</sub>-6.7, JB<sub>Jan</sub>-6.8 and JB<sub>Jan</sub>-6.9). The simulations at these sites  
 642 show the three lowest simulated  $T_B$  at 11 GHz and 19 GHz at H-pol (Fig. 11). The second  
 643 observed ice lens inserted in DMRT-ML significantly decreases the simulated  $T_B$ .  
 644 Including the second observed ice lens allows an improvement in the  $T_B$  simulation at  
 645 JB<sub>Jan</sub>-6.8 (Table 1), while the accuracy decreases for the two other snowpits, especially at  
 646 11 GHz. These results show the importance of small-scale spatial variability in the  
 647 distribution of ice lenses. In this case, since the SBR footprint is not exactly where the  
 648 snowpit was dug, the 11 GHz measured the two ice lenses at JB<sub>Jan</sub>-6.8, but not at JB<sub>Jan</sub>-  
 649 6.7 and JB<sub>Jan</sub>-6.9. Rutter et al. (2013) showed that such small-scale discontinuities in ice  
 650 lenses have a strong impact on  $T_B$ .  
 651



652  
 653 **Fig. 11.**  $T_B$  sensitivity associated with the  $\rho_{IL}$  variation (700 to 917 kg m<sup>-3</sup>).

654

655 **Table 11.**  $T_B$  sensitivity ( $\Delta T_B \rho_{IL}$ :  $T_B \rho_{IL917} - T_B \rho_{IL700}$ ) (K) associated with the  $\rho_{IL}$  variation  
 656 (700 to 917 kg m<sup>-3</sup>)

|     | JB <sub>Jan</sub> | JB <sub>Feb</sub> | JB <sub>Mar</sub> | UMI  |
|-----|-------------------|-------------------|-------------------|------|
| 11H | 17                | 15.9              | 11.9              | 13.4 |
| 11V | 3.7               | 3.1               | 2.6               | 3.5  |
| 19H | 15.4              | 14.3              | 9.2               | 12.1 |
| 19V | 3.2               | 2.4               | 1.8               | 3.1  |
| 37H | 6.4               | 5.7               | 1.2               | 6.1  |
| 37V | 0.8               | 1.5               | 1.7               | 1.1  |

657

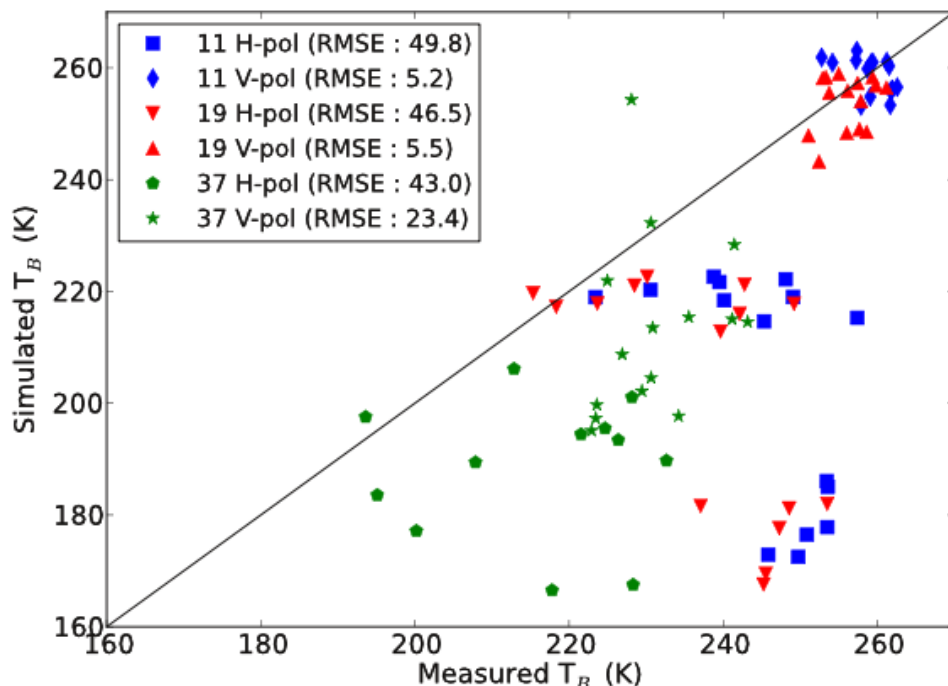
658

659 **3.2.5 Surrounding vegetation effects**

660

661 In a forested area, tree emission reflected by the snowpack can significantly contribute to  
 662 the measured  $T_B$  on the ground (Roy et al., 2012). An analysis was conducted on 18 site  
 663 measurements taken in a forest during the three James Bay campaigns (Table 4) to  
 664 quantify the forest contributions to measured  $T_B$  using DMRT-ML. A first simulation,  
 665 neglecting the emission coming from the trees in the downwelling  $T_B$  ( $T_{B\text{down}}$ ) reflected  
 666 by the surface was conducted. Figure 12 shows a clear underestimation (biases  $\approx 40$  K at  
 667 H-pol) of simulated  $T_B$  at all frequencies, except for 11 and 19 GHz at V-pol. Table 12  
 668 shows that these biases are much greater than the uncertainties induced by the snow cover  
 669 in open areas, showing that the tree emission reflected by the surface significantly  
 670 increased the measured  $T_B$ . The low influence of vegetation (low  $\text{bias}_{\text{forest}}$ : Table 12) at 11  
 671 and 19 GHz V-pol is explained by the fact that the reflectivity of the surface at these  
 672 frequencies is very low because the volume scattering is weak and the reflectivity at the  
 673 interfaces is close to zero near the Brewster angle.

674



675

676 **Fig. 12.** Simulated  $T_B$  in forested sites neglecting the vegetation contribution ( $T_{B\text{down}}$ ).

677

678

679 **Table 12.** Comparison between the calculated biases in an open area and in a forested  
area

|     | $\text{Bias}_{\text{open}}$ | $\text{Bias}_{\text{forest}}$ |
|-----|-----------------------------|-------------------------------|
| 11H | 4.7                         | -41.7                         |
| 11V | -4.0                        | -1.1                          |

|     |      |       |
|-----|------|-------|
| 19H | -4.0 | -35.9 |
| 19V | -5.7 | -3.4  |
| 37H | 2.2  | -37.4 |
| 37V | 3.3  | -21.4 |

680 To quantify the forest contribution, the  $T_{B\text{down}}$  was inverted with DMRT-ML. From the  
 681 simulated  $T_B$  neglecting the forest contribution (Fig. 12), an iteration process was  
 682 performed to find the  $T_{B\text{down}}$  value that minimized the  $\text{RMSE}_{\text{veg}}$  between simulated and  
 683 measured  $T_B$  at V-pol and H-pol for each frequency independently:  
 684

$$685 \quad \text{RMSE}_{\text{veg}} = \sqrt{\frac{\sum_{i=1}^N (T_{B\text{sim};i}^{fV} - T_{B\text{mes};i}^{fV})^2 + (T_{B\text{sim};i}^{fH} - T_{B\text{mes};i}^{fH})^2}{2N}} \quad (6)$$

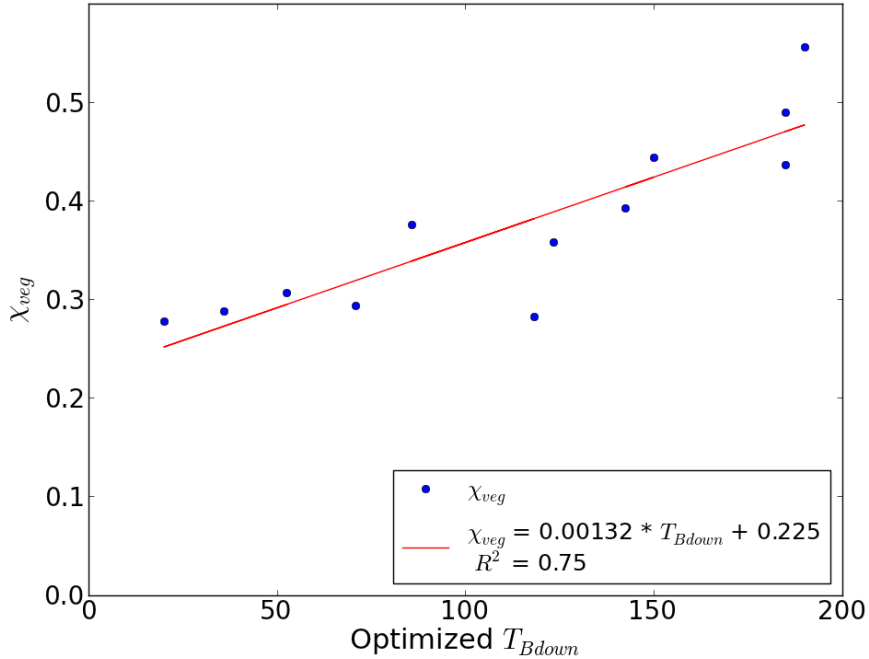
687 where  $f$  is the frequency.  
 688

689 Table 13 shows that the averaged optimized  $T_{B\text{down}}$  are 147 K, 120 K and 110 K  
 690 respectively at 11, 19 and 37 GHz. The optimized  $T_{B\text{down}}$ , however, decrease with  
 691 frequency, which is opposite to what was shown in other studies (Kruopis et al., 1999;  
 692 Roy et al., 2012; Roy et al., 2014). This is probably related to the inherent error in the  
 693 snow surface  $T_B$  simulation in DMRT-ML (Table 7), which induces error in the  
 694 calculation of the reflectivity of the snow-covered surface.  
 695

696 **Table 13.** Average optimized  $T_{B\text{down}}$  and standard deviation (in parentheses) (K)

|                        | 11 GHz           | 19 GHz           | 37 GHz           |
|------------------------|------------------|------------------|------------------|
| $T_{B\text{down}}$ (K) | 147 ( $\pm 64$ ) | 120 ( $\pm 74$ ) | 110 ( $\pm 43$ ) |

698 Table 13 also shows that there are large variations between the different snowpits with a  
 699 standard deviation between 43 K and 74 K. The average  $T_{B\text{down}}$  of the three frequencies  
 700 was calculated for each site and compared with  $\chi_{\text{veg}}$  obtained from fisheye pictures taken  
 701 at the twelve  $JB_{\text{veg}}$  sites in January and February (fisheye pictures were not taken in  
 702 March). Figure 13 shows that there is a good correlation ( $R^2 = 0.75$ ) between averaged  
 703  $T_{B\text{down}}$  (mean for the three frequencies) and  $\chi_{\text{veg}}$ . These results confirm that the optimized  
 704  $T_{B\text{down}}$  are related to the tree emission reflected by the surface (see an example of  
 705 variations in Fig. 1). For comparison, the calculated atmospheric downwelling  
 706 contributions were around 6 K at 11 GHz and 25 K at 37 GHz. It also shows the potential  
 707 of using fisheye pictures to quantify tree microwave emission in boreal forests. However,  
 708 further considerations are necessary to improve the method. Because of the non-  
 709 Lambertian component of the snow reflection and the non-homogeneity of the trees  
 710 surrounding the site measurements, the direction (azimuth) in which the SBR is pointing  
 711 has an important influence on the signal (Courtemanche et al., 2015). DMRT-ML  
 712 assumed that the  $T_{B\text{down}}$  is isotropic, and does not take into account these specular  
 713 components. For example, the  $T_B$  will be higher if the SBR is pointing in the direction of  
 714 a large trunk close to the snowpit instead of pointing in the direction of a forest opening.  
 715



716  
717 **Fig. 13.** Relationship between the average  $T_{B\text{down}}$  of the three frequencies and the  
718 proportion of pixels occupied by vegetation (trees) in the fisheye pictures ( $\chi_{\text{veg}}$ ) for the 12  
719 JB<sub>veg</sub> sites in January and February.

720  
721 **4. Discussion / conclusion**

722 This study presents a comprehensive analysis of the [geophysical parameters](#) contributing  
723 to uncertainty in DMRT-ML for snow-covered surfaces in boreal forest, subarctic and  
724 arctic environments. A unique in situ database, including key information on the  
725 snowpack temporal winter evolution, allowed the assessment of the impact of spatial  
726 variability of 1) soil emission, 2) errors in snow grains and 3) density measurements, 4)  
727 ice lenses and 5) vegetation emission reflected from the surface on DMRT-ML  
728 simulations.

729  
730 The implementation in DMRT-ML of the bridging aiming at filling the gap between low  
731 and high snow density ranges where the theory is invalid has been tested. Bridging leads  
732 to a small improvement for tundra snow where wind slabs are present. These  
733 improvements are modest and could compensate for the measurement uncertainties or  
734 other limitations related to the use of the model such as stickiness and grain size  
735 distribution (Roy et al., 2013). Based on the work of Dierking et al. (2012), the range of  
736 the ice fraction where bridging was applied was limited to 0.4 - 0.6, but could be  
737 extended and lead to a stronger impact of bridging on the results (Tsang et al., 2008). But  
738 as shown in this study, the uncertainties in measurements make it difficult to make sure  
739

740 that any optimization of the bridging range does not compensate for other uncertainties.  
741 In practice, this new version of DMRT-ML with bridging facilitates simulation of snow  
742 and/or ice without identification of the snow layer state.

743  
744 Based on several snow removal experiments, the study shows that small-scale variability  
745 in soil emissivity in a boreal forest has a second order effect on the snow-covered surface  
746  $T_B$  when the soil is frozen, even for lower frequencies that are more transparent to the  
747 snowpack (11 and 19 GHz). In practice, this implies that the use of constant soil  
748 parameters for frozen soil emission modeling for a given environment is adequate for  
749 snow emission studies. This result is surprising since soil roughness, soil wetness,  
750 freeze/thaw state and stratigraphy are usually difficult to measure in boreal conditions.  
751 However, further experiments should be done to validate this aspect for other types of  
752 environments. Exploring larger scales could help to determine at what scale soil  
753 emissivity has an influence on snow-covered  $T_B$ .  
754

755 This study shows the strong sensitivity of DMRT-ML to snow grain size and density at  
756 37 GHz, and that the error related to the measurements can explain most of the RMSE at  
757 this frequency and probably at higher frequencies. These results are in agreement with  
758 studies using MEMLS (Durand et al., 2008) and HUT (Rutter et al., 2013; Lemmetynen  
759 et al., 2015). It remains difficult to distinguish the sources of error related to DMRT-ML  
760 simulations at 37 GHz. The study, however, underlines that measurement error limits the  
761 accuracy of the simulations. The error related to the physical simplifications in DMRT-  
762 ML was not investigated in this work, but our results suggest that the level of confidence  
763 of measurements is too low to test or significantly improve the DMRT-ML physics. **In**  
764 **this study, SSA was used because it is a robust and objective metric that can be measured**  
765 **effectively on the field. However, the derived  $R_{opt}$  metric used in DMRT-ML is related to**  
766 **an optical definition (Grenfell and Warren, 1999) and might not represent the grain for**  
767 **microwave wavelength (Mätzler, 2002).** Further experiments on isolated snow layers as  
768 done by Wiesmann et al. (1998) but using new tools for snow microstructure  
769 parameterization could be applied to improve the physics of emission models. For  
770 example, more precise measurements of snow microstructure like X-ray tomography  
771 (Heggli et al., 2011) and the snow micro penetrometer (SMP) (Schneebeli et al., 1999;  
772 Proksch et al., 2015) could be the next step to improve the understanding of the physics  
773 in DMRT-ML (e.g., Lowe and Picard, 2015). However, each snow microstructure  
774 measurement method has its own limitations. Combining the different information could  
775 be an avenue to better quantify the snow scattering mechanism in DMRT-ML.

776 This analysis confirms that the scaling factor ( $\phi = 3.3$ ) proposed by Roy et al. (2013) is a  
777 general value as it yields accurate results with the new data set presented in this paper.  
778 We do not pretend that this value exactly applies to other environments as Picard et al.  
779 (2014) found a lower value (2.3) for Antarctica with a SSA measurement technique that  
780 was inter-calibrated with ours. The temporal analysis during the three campaigns in  
781 James Bay, however, shows that the sensitivity to snow measurement uncertainties  
782 evolve during winter due to snow metamorphism. This sensitivity change is also  
783 important at 19 GHz. Although snow is almost transparent at this frequency at the  
784 beginning of winter when the grains are small,  $T_B$  at 19 GHz becomes sensitive to snow  
785 in March because of snow grain growth. This could be of interest for the SWE retrieval

786 approach, knowing that 19 GHz  $T_B$  becomes sensitive to snow when snow grains become  
787 larger. **As proposed in Derksen (2008) 11 and 19 GHz frequencies could be usefull for**  
788 **SWE retrievals for deep snow to overcome the problem of saturation at 37 GHz (see**  
789 **Rosenfeld and Grody, 2000).** At 11 GHz, snow is almost transparent throughout the  
790 winter demonstrating the utility of this band for monitoring soil conditions (phase,  
791 temperature) under the snow (Kohn and Royer, 2010).

792  
793 The inclusion of ice lenses in DMRT-ML significantly improves the simulations at H-  
794 pol. However, the model is not able to reproduce the observed spatial variability at 11  
795 and 19 GHz at H-pol, which was shown to be related to snowpack stratigraphy  
796 inaccuracies, mostly related to ice lenses and strong variations in snow density (for  
797 example, thin snow crust). The large spatial variability of ice lenses and snow crusts at  
798 the meter scale (Rutter et al., 2013) can lead to the strong spatial variability of observed  
799  $T_B$ . This ice lenses and snow crust spatial variability raise the need to develop efficient  
800 and practical methods to effectively characterize ice lenses and thin snow crusts,  
801 especially their density (Marsh and Woo, 1984). Using short-wave infrared photography  
802 (Montpetit et al., 2012) or SMP profiles (Proksch et al., 2015) are possible options. The  
803 coherence, which is not taken into account in DMRT-ML, is responsible for a large  
804 sensitivity of  $T_B$  to ice lens thickness and can explain the observed  $T_B$  variability at 19  
805 and 11 GHz at H-pol. The implementation of the coherence in DMRT-ML is not difficult,  
806 but collecting the input variables in the field remains the major challenge.

807  
808 In boreal forest areas, our analysis shows that the vegetation emission reflected by the  
809 snow-covered surface can contribute more than 200 K and that neglecting the reflection  
810 of the signal on the snow surface can lead to a bias of up to 40 K, mostly at H-pol where  
811 the surface reflectivity is the highest. This bias is coupled to the snow state, depending on  
812 the snow reflectivity. These results clearly show the importance of the vegetation  
813 contribution and avoiding this contribution in measurements imply to operate in clearings  
814 with minimal forest cover mostly on the opposite side of the measurements (specular  
815 contributions). However, some promising results on the use of fisheye photographs to  
816 quantify that vegetation contribution were shown. The use of a Lambertian microwave  
817 surface for retrieving the downwelling contribution in ground-based radiometric  
818 measurements (Courtemanche et al., 2015) may also be a promising avenue.

819  
820 To the best of our knowledge, this is the first time that an analysis has been carried out of  
821 all the elements (soil, grain size, snow density, ice lenses, and vegetation) that contribute  
822 to the microwave signal at three frequencies (36.5, 18.7 and 10.65 GHz) in a boreal  
823 forest. The study sheds light on DMRT-ML uncertainties related to small-scale variability  
824 and measurement errors in different environments and for different periods in the winter.  
825 Some limitations were raised on the accuracy of DMRT-ML to simulate the  $T_B$  of snow-  
826 covered surfaces, and this analysis will help to design future studies to improve the  
827 ability of DMRT-ML and other MESM to model the radiative transfer processes of snow-  
828 covered surfaces.

829  
830  
831 *Acknowledgements*

832  
833 The authors would like to thank the National Sciences and Engineering Research Council  
834 of Canada (NSERC) and Environment Canada for their financial support. The French  
835 collaboration was supported by the Programme de développement de partenariats  
836 stratégiques en matière d'enseignement et de recherche (FRQNT- Conseil franco-  
837 québécois de la coopération universitaire); Patrick Cliche, Serge Langlois, Nathalie  
838 Thériault, Caroline Dolant and Bruno-Charles Busseau (Université de Sherbrooke), Éric  
839 Lefebvre (Laboratoire de glaciologie et géophysique de l'environnement de Grenoble),  
840 Bernard Lesaffre (CNRM-GAME, MétéoFrance-CNRS) and Florent Dominé and  
841 Mathieu Barrère (Takuvik and Université Laval) for their contributions to the field work  
842 to obtain these measurements; Peter Toose and Chris Derksen (Environment Canada) for  
843 providing part of Churchill data. The French polar institute (IPEV) has contributed  
844 through the BIPOL project. We also thank Élie Girard, Université de Sherbrooke, for his  
845 contributions in data processing and simulations. We would like to thanks the two  
846 anonymous reviewers for their helpful comments.  
847  
848

## 849 **References**

850  
851 Armstrong, R. L., and Brun, E.: Snow and Climate: Physical Processes, Surface Energy  
852 Exchange and Modeling, Cambridge University Press, 222 pp., 2008.  
853  
854 Brucker, L., Picard, G., Arnaud, L., Barnola, J.-M., Schneebeli, M., Brunjail, H.,  
855 Lefebvre, E., and Fily, M.: Modelling time series of microwave brightness temperature at  
856 Dome C, Antarctica, using vertically resolved snow temperature and microstructure  
857 measurements, *J. Glaciol.*, 57, 171–182, 2011.  
858  
859 Champollion, N., Picard, G., Arnaud, L., Lefebvre, E., and Fily, M.: Hoar crystal  
860 development and disappearance at Dome C, Antarctica: observation by near-infrared  
861 photography and passive microwave satellite, *The Cryosphere*, 7, 1247–1262,  
862 doi:10.5194/tc-7-1247-2013, 2013.  
863  
864 Chang, A. T. C., Foster, J. L., and Hall, D. K.: Nimbus-7 SMMR derived  
865 global snow cover parameters, *Ann. Glaciol.*, 9, 39–44, 1987.  
866  
867 Colbeck, S.: Theory of metamorphism of dry snow, *J. Geophys. Res.*, 88, 5475–5482,  
868 1983.  
869  
870 Courtemanche, B., Montpetit, B., Royer, A., and Roy, A.: Creation of a Lambertian  
871 microwave surface for retrieving the downwelling contribution in ground-based  
872 radiometric measurements, *IEEE T. Geosci. Remote*, 12, 462–466, 2015.  
873  
874 Derksen, C.: The contribution of AMSR-E 18.7 and 10.7 GHz measurements to improved  
875 boreal forest snow water equivalent retrievals, *Remote Sens. Environ.*, 112, 2701–2710,  
876 2008.  
877

878 Derksen, C., Toose, P., Lemmetyinen, J., Pulliainen, J., Langlois, A., Rutter, N., and  
879 Fuller, M.: Evaluation of passive microwave brightness temperature simulations and  
880 snow water equivalent retrievals through a winter season, *Remote Sens. Environ.*, 117,  
881 236–248, 2012.

882

883 Déry, S. J., Hernandez-Henriquez, M. A., Burford, J. E., and Wood, E. F.: Observational  
884 evidence of an intensifying hydrological cycle in the northern Canada, *Geophys. Res.*  
885 *Lett.*, 36, L13402, 2009.

886

887 Dierking, W., Linow, S., and Rack, W.: Toward a robust retrieval of snow accumulation  
888 over the Antarctic ice sheet using satellite radar, *J. Geophys. Res.*, 117, D09110,  
889 doi:10.1029/2011JD017227, 2012

890

891 Dupont, F., Picard, G., Royer, A., Fily, M., Roy, A., Langlois, A., and Champollion, N.:  
892 Modeling the microwave emission of bubbly ice: applications to blue ice and  
893 superimposed ice in the Antarctic and Arctic, *IEEE T. Geosci. Remote*, 52, 6639–6651,  
894 2014.

895

896 Durand, M., Kim, E. C., and Margulis, S.: Quantifying uncertainty in modeling snow  
897 microwave radiance for a mountain snowpack at the point-scale, including stratigraphic  
898 effects, *IEEE T. Geosci. Remote*, 46, 1753–1767, 2008.

899

900 Gallet, J.-C., Domine, F., Zender, C. S., and Picard, G.: Measurement of the specific  
901 surface area of snow using infrared reflectance in an integrating sphere at 1310 and 1550  
902 nm, *The Cryosphere*, 3, 167–182, doi:10.5194/tc-3-167-2009, 2009.

903

904 Goodison, B., Rubinstein, I., Thirkettle, F., Langham, E.: Determination of snow water  
905 equivalent on the Canadian Prairies using microwave radiometry, *Proc. of the Budapest*  
906 *Symposium*, 163–173, 1986.

907

908 Gouttevin, I., Menegoz, M., Dominé, F., Krinner, G., Koven, C., and Ciais, P.: How the  
909 insulating properties of snow affect soil carbon distribution in the continental pan-Arctic  
910 area, *J. Geophys. Res.*, 117, G02020, 2012.

911

912 Grenfell, T. C., and Warren, S. G.: Representation of a nonspherical ice particle by  
913 collection of independent spheres for scattering and absorption of radiation, *J. Geophys.*  
914 *Res.*, 104, 31697–31709, 1999.

915

916 Latifovic, R., Zhu, Z.-L., Cihlar, J., Giri, C., and Olthof, I.: Land cover mapping of North  
917 and Central America – Global land cover 2000. *Remote Sens. Environ.*, 89, 116–127,  
918 2004.

919

920 Liston, G. E., McFadden, J. P., Sturm, M., and Pielke, R. A.: Modelled changes in arctic  
921 tundra snow, energy and moisture fluxes due to increased shrubs, *Glob. Change Biol.*, 8,  
922 17–32, 2002.

923

924 Heggli, M., Köchle, B., Matzl, M., Pinzer, B.R., Riche, F., Steiner, S., Steinfeld, D.,  
925 and Schneebeli, M.: Measuring snow in 3-D using X-ray tomography: assessment of  
926 visualization techniques, *Ann. Glaciol.*, 52, 231–236, 2011.

927

928 Jin, Y.: Electromagnetic Scattering Modelling for Quantitative Remote Sensing.  
929 Singapore: World Scientific, 1994.

930

931 Kokhanovsky, A. A. and Zege, E. P.: Scattering optics of snow, *Appl. Optics*, 43, 1589–  
932 1602, 2004.

933

934 Kohn, J., and Royer, A.: AMSR-E data inversion for soil temperature estimation under  
935 snow cover, *Remote Sens. Environ.*, 114, 2951–2961, 2010.

936

937 Kontu, A. and Pulliainen, J.: Simulation of spaceborne microwave radiometer  
938 measurements of snow cover using in situ data and brightness temperature modeling,  
939 *IEEE T. Geosci. Remote*, 48, 1031–1044, 2010.

940

941 Kruopis, N., Praks, J., Arslan, A. N., Alasalmi, H. M., Koskinen, J. T., and Hallikainen,  
942 M. T.: Passive microwave measurements of snow-covered forest area in EMAC'95. *IEEE*  
943 *T. Geosci. Remote*, 37, 2699–2705, 1999.

944

945 Langlois, A.: Applications of the PR series radiometers for cryospheric and soil moisture  
946 research, Radiometrics Corporation, 40 pp., 2015.

947

948 Larue, A., Royer, A., De Sève, D., Langlois, A., and Roy, A.: Validation analysis of the  
949 GlobSnow2 database over an eco-climatic latitudinal gradient in Eastern Canada, *J.*  
950 *Hydrometeorol.*, in redaction, 2015.

951

952 Lemmetyinen, J., Pulliainen, J., Rees, A., Kontu, A., Qiu, Y., and Derksen, C.: Multiple-  
953 layer adaptation of HUT snow emission model: Comparison with experimental data,  
954 *IEEE T. Geosci. Remote*, 48, 2781–2794, 2010.

955

956 Lemmetyinen, J., Derksen, D., Toose, P., Proksh, M., Pulliainen, J., Kontu, A.,  
957 Rautiainen, K., Seppänen, J., Hallikainen, M.: Simulating seasonally and spatially  
958 varying snow cover brightness temperature using HUT snow emission model and  
959 retrieval of a microwave effective grain size, *Remote Sens. Environ.*, 156, 71–95, 2015.

960

961 Lemmetyinen, J., Schwank, M., Rautiainen, K., Kontu, A., Parkkinen, T., Mätzler, C.,  
962 Wiesmann, A., Wegmüller, U., Derksen, C., Toose, P., Roy, A., and Pulliainen, J.: Snow  
963 density and ground permittivity retrieved from L-Band radiometry: application to  
964 experimental data, *Remote Sens. Environ.*, In review, 2015.

965

966 Liebe, H.: MPM—An atmospheric millimeter-wave propagation model, *Int. J. Infrared*  
967 *Millim. Waves*, 10, 631–650, 1989.

968

969 Löwe, H. and Picard, G.: Microwave scattering coefficient of snow in MEMLS and

970 DMRT-ML revisited: the relevance of sticky hard spheres and tomography-based  
971 estimates of stickiness, *The Cryosphere Discuss.*, 9, 2495–2542, doi:10.5194/tcd-9-2495-  
972 2015, 2015.

973

974 Marsh, P., and Woo, M.-K.: Wetting front advance and freezing of meltwater within a  
975 snow cover 1. Observations in the Canadian arctic, *Water Resour. Res.*, 20, 1853–1864,  
976 1984.

977

978 Mätzler, C.: Relation between grain-size and correlation length of snow, *J. Glaciol.*, 48,  
979 461–466, 2002.

980

981 Mätzler, C.: Applications of the interaction of microwaves with natural snow cover,  
982 *Remote Sens. Rev.*, 2, 259–392, 1987.

983

984 Mesinger, F., Dimego, G., Kalnay, E., Mitchell, K., Shafran, P. C., Ebisuzaki, W., Jovic,  
985 D., Woollen, J., Rogers, E., Berbery, E. H., Ek, M. B., Fan, Y., Grumbine, R., Higgins,  
986 W., Li, H., Lin, Y., Manikin, G., Parrish, D. and Shi, W.: North American regional  
987 reanalysis, *Bull. Amer. Meteorol. Soc.*, 87, 343–360, 2006.

988

989 Montpetit, B., Royer, A., Langlois, A., Cliche, P., Roy, A., Champollion, N., Picard, G.,  
990 Domine, F., and Obbard, R.: New shortwave infrared albedo measurements for snow  
991 specific surface area retrieval, *J. Glaciol.*, 58, 941,  
992 doi:10.1016/j.coldregions.2010.01.004, 2012.

993

994 Montpetit, B., Royer, A., Roy, A., Langlois, L., and Derksen, D.: Snow microwave  
995 emission modeling of ice lenses within a snowpack using the microwave emission model  
996 for layered snowpacks, *IEEE T. Geosci. Remote*, 51, 4705–4717,  
997 doi:10.1109/TGRS.2013.2250509, 2013.

998

999 Montpetit, B.: Analyse de la modélisation de l'émission multi-fréquences micro-ondes et  
1000 de la neige, incluant les crottes de glace à l'aide du modèle Microwave Emission Model  
1001 of Layered Snowpack (MEMLS), Ph.D thesis, Université de Sherbrooke, 168 pp,  
1002 <http://hdl.handle.net/11143/6844>.

1003

1004 Picard, G., Brucker, L., Roy, A., Dupont, F., Fily, M., and Royer, A.: Simulation of the  
1005 microwave emission of multi-layered snowpacks using the dense media radiative transfer  
1006 theory: the DMRT-ML model, *Geosci. Model Dev. Discuss.*, 5, 3647–3694,  
1007 doi:10.5194/gmdd-5-3647-2012, 2012.

1008

1009 Picard, G., Royer, A., Arnaud, L., and Fily, M.: Influence of meter-scale wind-formed  
1010 features on the variability of the microwave brightness temperature around Dome C in  
1011 Antarctica, *The Cryosphere*, 8, 1105–1119, doi:10.5194/tc-8-1105-2014, 2014.

1012

1013 Proksch, M., Löwe, H., and Schneebeli, M: Density, specific surface area, and correlation  
1014 length of snow measured by high-resolution penetrometry, *J. Geophys. Res. Earth Surf.*,  
1015 120, 346–362, doi:10.1002/2014JF003266, 2015.

1016  
1017 Rees, A., Lemmetyinen, J., Derksen, C., Pulliainen, J. T., and English, M.: Observed and  
1018 modelled effects of ice lens formation on passive microwave brightness temperatures  
1019 over snow covered tundra, *Remote Sens. Environ.*, 114, 116–126, 2010.  
1020  
1021 Rosenfeld, S., and Grody, N.: Anomalous microwave spectra of snow cover observed  
1022 from Special Sensor Microwave/Imager measurements, *J. Geophys. Res.*, 105, D11,  
1023 14913–14925, 2000.  
1024  
1025 Roy, A., Royer, A., and Turcotte, R.: Improvement of springtime streamflow simulations  
1026 in a boreal environment by incorporating snow-covered area derived from remote sensing  
1027 data, *J. Hydrol.*, 390, 35–44, 2010.  
1028  
1029 Roy, A., Royer, A., Wigneron, J.-P., Langlois, A., Bergeron, J., and Cliche, P.: A simple  
1030 parameterization for a boreal forest radiative transfer model at microwave frequencies,  
1031 *Remote Sens. Environ.*, 124, 371–383, 2012.  
1032  
1033 Roy, A., Picard, G., Royer, A., Montpetit, B., Dupont, F., Langlois, A., Derksen, C., and  
1034 Champollion, N.: Brightness temperature simulations of the Canadian seasonal snowpack  
1035 driven by measurements of the snow specific surface area, *IEEE T. Geosci. Remote*, 51,  
1036 4692–4704, doi:10.1109/TGRS.2012.2235842, 2013.  
1037  
1038 Roy, A., Royer, A., and Hall, J. R.: Relationship between forest microwave  
1039 transmissivity and structural parameters for the Canadian boreal forest, *Geophys. Res.*  
1040 *Lett.*, 11, 1802–1806, 2014.  
1041  
1042 Roy, A., Royer, A., Montpetit, B., and Langlois, A.: Microwave snow emission modeling  
1043 of boreal forest environments, *Proc. IGARSS2015*, Milan, Italy, July, 754–757, 2015.  
1044  
1045 Rutter, N., Sandells, M., Derksen, C., Toose, P., Royer, A., Montpetit, B., Langlois, A.,  
1046 Lemmetyinen, J., and Pulliainen, J.: Snow stratigraphic heterogeneity within ground-  
1047 based passive microwave radiometer footprints: Implications for emission modeling, *J.*  
1048 *Geophys. Res. Earth Surf.*, 119, 550–565, doi:10.1002/2013JF003017, 2013.  
1049  
1050 Schneebeli, M., Pielmeier, C., and Johnson, J.: Measuring snow microstructure and  
1051 hardness using a high resolution penetrometer, *Cold Reg. Sci. Technol.*, 30, 101–114,  
1052 doi:10.1016/S0165-232X(99)00030-0, 1999.  
1053  
1054 Schuur, E. A. G., Abbott, B.W., Bowden, W.B., Brovkin, V., Camill, P., and Canadell,  
1055 J.G.: Expert assessment of vulnerability of permafrost carbon to climate change. *Clim.*  
1056 *Change*, 119, 359–374, 2013.  
1057  
1058 Takala, M., Luojus, K., Pulliainen, J., Derksen, C., Lemmetyinen, J., Kärnä, J.-P., and  
1059 Koskinen, J.: Estimating northern hemisphere snow water equivalent for climate research  
1060 through assimilation of space-borne radiometer data and ground-based measurements,  
1061 *Remote Sens. Environ.*, 115, 3517–3529, 2011.  
1062

1063 Tedesco, M., and Kim, E. J.: Intercomparison of electromagnetic models for passive  
1064 microwave remote sensing of snow, *IEEE T. Geosci. Remote*, 44, 2654–2666, 2006.

1065

1066 Tsang, L., Kong, J. A., Ding, K.-H., and Ao C. O.: *Scattering of Electromagnetic Waves: Numerical Simulations*. New York, NY, USA: Wiley, 2001.

1067

1068 Tsang, L., Liang, D., Xu, X., and Xu, P.: Microwave emission from snowpacks: Modeling the effects of volume scattering, surface scattering and layering, in *Proc. 10<sup>th</sup> Spec. Meet. Microw. Radiometry Remote Sens. Environ. (MicroRad)*, Firenze, Italy, Mar. 11–14, pp.1–4, 2008.

1069

1070

1071

1072

1073

1074 Wegmüller, U., and Mätzler, C.: Rough bare soil reflectivity model, *IEEE T. Geosci. Remote.*, 37, 1391–1395, 1999.

1075

1076

1077 Wiesmann, A., Mätzler, C., and Weise, T.: Radiometric and structural measurements of snow samples, *Radio Sci.*, 33, 273–289, 1998.

1078

1079